Progress of Theoretical Physics, Vol. 70, No. 1, July 1983

Light p-Shell Λ-Hypernuclei by the Microscopic Three-Cluster Model

Toshio MOTOBA, Hiroharu BANDŌ* and Kiyomi IKEDA**

Laboratory of Physics, Osaka Electro-Communication University, Neyagawa, Osaka 572
**Division of Mathematical Physics, Fukui University, Fukui 910*
***Department of Physics, Niigata University, Niigata 950-21*

(Received march 7, 1983)

A systematic investigation of ${}^{6}_{\Lambda}$He, ${}^{6}_{\Lambda}$Li, ${}^{7}_{\Lambda}$Li, ${}^{8}_{\Lambda}$Li and ${}^{9}_{\Lambda}$Be hypernuclei is carried out within the framework of the microscopic $\alpha+x+\Lambda$ cluster-model dynamics ($x=n, p, d, t$ or α). The positive and negative parity energy spectra are analysed in detail and are classified into several characteristic "bands" according to the underlying structures. The E2, E1 and M1 γ-ray transition probabilities and magnetic dipole moments are calculated. The intra-band B(E2)'s are obtained to be several times enhanced in comparison with the shell-model values. The level widths of the strong peaks observed at lower B_Λ are roughly evaluated on the basis of the calculated reduced width amplitudes. The existing data can be well explained by the present model. The cluster-model estimates of the effective neutron number $N_{\rm eff}(\theta=0°)$ for the (K^-, π^-) reaction are consistent with the experiments.

§ 1. Introduction

Recent experiments[1)~9)] on the strangeness exchange (K, π) reaction have been providing the important information on excited states of Λ(and Σ)-hypernuclei. This adds to the ground state energy data previously given by emulsion experiments. Following a series of epoch-making works done in CERN by the Heidelberg-Saclay-Strasbourg group,[1)~5)] measurements of the pion angular distribution and associated transition γ-rays in (K, π) reactions started in Brookhaven.[6)~9)] These experiments seem to have opened a gate to the hypernuclear spectroscopy which is expected to disclose dynamical aspects of the hypernuclear structure. In such a status of experimental works, theoretical investigations are required to be accordingly leveled up, so that predictions of various physical quantities can be made in necessary details.

Hypernuclei have been investigated from a variety of viewpoints.[5),10)~18)] The structure of light hypernuclei attracts particular interests because of their individual characters. Even a single hyperon added to light nuclei will be able to reveal new and genuinely hypernuclear aspects. In fact relatively rich data have been accumulated on light hypernuclei. The purpose of this paper is to perform a systematic study of light "p-shell" Λ-hypernuclei listed in Table I.[19)]

Since more than ten years ago, Gal, Soper and Dalitz[11),15)] have made extensive applications of the shell model to p-shell Λ-hypernuclei within the configuration $(0s)_N{}^4(0p)_N{}^{A-5}(0s)_\Lambda$. Recently the $SU(3)$ group classification has been applied to $A=9$ -13 hypernuclear spectra by Zhang et al.[20)] and to ${}^{9}_{\Lambda}$Be by Dalitz and Gal.[21)] An extended shell-model calculation has been carried out by Majling et al.[22)] for the ${}^{6}_{\Lambda}$Li case by including higher configurations. Auerbach et al.[23)] have successfully interpreted the observed low-lying spectrum of ${}^{13}_{\Lambda}$C by employing the shell model on the basis of Cohen-Kurath wave functions. On the other hand, in the 1960's ground states of some of these

Table I. Alpha and "x" clusters composing the light p-shell nuclei and Λ-hypernuclei. $S_x + S_\Lambda(1/2) = S$.

	"$\alpha+x$"	Spin(S_x)		"$\alpha+x+\Lambda$"	Spin(S)
^{5}He	$\alpha+n$	1/2	$^6_\Lambda$He	$\alpha+n+\Lambda$	0, 1
^{5}Li	$\alpha+p$	1/2	$^6_\Lambda$Li	$\alpha+p+\Lambda$	0, 1
^{6}Li	$\alpha+d$	1	$^7_\Lambda$Li	$\alpha+d+\Lambda$	1/2, 3/2
^{7}Li	$\alpha+t$	1/2	$^8_\Lambda$Li	$\alpha+t+\Lambda$	0, 1
^{8}Be	$\alpha+\alpha$	0	$^9_\Lambda$Be	$\alpha+\alpha+\Lambda$	1/2
(^{9}Be	$\alpha+\alpha+n$	1/2)			

Λ-hypernuclei were investigated by Dalitz and Rajasekaran,[24] Bodmer et al.[25),26] and Tang and Herndon[27),28] with the cluster model in which constituent clusters were treated as structureless particles. More recently Rēvai and Žofka[29] have applied a molecular three-body approach to study low-lying spectra of $^9_\Lambda$Be. The Faddeev equation approach has been made by Sunami and Narumi.[3] A fully microscopic $\alpha+\alpha+\Lambda$ three-cluster model has been exploited by one of the present authors with Seki and Shono (BSS)[31] to extensively investigate the structure characteristics of $^9_\Lambda$Be.

The approach used in this paper lies on the line of the BSS model[31] with some natural generalization. In the hypernuclei which we treat, the cluster aspect is believed to be important, as it is so in the corresponding ordinary nuclei.[32),33] It is thus necessary to incorporate both the shell-model and cluster-model aspects. This is the reason why we treat the hypernuclei under consideration as a microscopic $\alpha+x+\Lambda$ ($x=n$, p, d, t or α) three-body problem. In this model the α and x clusters are treated to be composite and the antisymmetrization among all nucleons are properly taken into account. The cluster-model wave functions can include not only usual low-lying configurations but also particular types of higher shell-model configurations without any spurious center-of-mass excitation. This is essential to the realistic prediction of electromagnetic transition probabilities and particle-decay widths as well as energy properties. What to use as the effective N-N and Λ-N interactions is another important point for the model. The basic baryon-baryon interaction has complicated properties coming from various meson exchanges, such as the repulsive core, non-central force, coupling with other baryon channels and so forth. These properties should somehow persist in the effective interaction in hypernuclei. In this paper, however, we purposely choose the use of quite simple effective interactions, because the principal aim at the present stage is to establish the basic feature of the hypernuclear structure.

In § 2 the microscopic three-cluster model is formulated. We treat a variety of states where the Λ particle and/or the core nucleus are allowed to be excited. The channel-coupled secular equation is obtained and the orthogonality-condition-model treatment for the α-x core nucleus part is also described. In the four subsections of § 3, the cluster-model expressions are respectively given for i) electric quadrupole and dipole transition probabilities, ii) magnetic dipole transition probability and moment, iii) reduced width amplitudes and spectroscopic factors going to the (αx)-Λ and $^5_\Lambda$He-x channels, and iv) effective neutron numbers for the (K^-, π^-) reactions. In § 4 the calculated results are presented and discussed individually for $^9_\Lambda$Be, $^8_\Lambda$Li, $^7_\Lambda$Li and $^6_\Lambda$He($^6_\Lambda$Li) in this order. The resultant energy levels are classified according to the underlying structural characteristics. Various physical quantities are predicted. Summary and concluding remarks are given in § 5.

§ 2. Formulation of the microscopic $\alpha+x+\Lambda$ three-cluster model

—— *Calculation of Energy Eigenvalues* ——

2.1. *Model wave functions and equation of motion*

By choosing the coordinate system shown in Fig. 1(a) the model wave function (wf) of a hypernucleus $(\alpha+x+\Lambda)$ with total angular momentum J is expanded as

$$\Psi_J=\sum_c\sum_{dK} w_c(d, K)|[\Phi(l, d)\times u_{K\lambda}(\boldsymbol{R})]_L[S_xS_\Lambda]_S; J\rangle, \tag{2·1}$$

where $c=\{l, \lambda, L, S\}$ denotes a channel of the angular momentum coupling, l and λ referring to the α-x and (αx)-Λ coordinates, respectively. Spins are denoted by S_x, S_Λ and totally S as seen in Table I. The relative wf between the Λ-particle and the center-of-mass of $\alpha+x$ nucleus is spanned by the normalized harmonic oscillator (ho) wf $u_{K\lambda}(\boldsymbol{R}) = u_{K\lambda}(R)Y_\lambda(\hat{\boldsymbol{R}})$, $K=2\nu+\lambda$ (K=number of ho quanta). The $\Phi(l; d)$ is the generator coordinate basis wf for the description of the $\alpha+x$ core nucleus;

$$\Phi(l; d)=\frac{1}{\sqrt{1+\delta_{\alpha x}}}\sqrt{\frac{4!x!}{(4+x)!}}\mathcal{A}'\{\phi_\alpha\,\phi_x\,\psi_l(r; d)Y_l(\hat{\boldsymbol{r}})\}, \tag{2·2}$$

$$\psi_l(r; d)=4\pi(\sqrt{\pi}\,b_r)^{-3/2}e^{-(r^2+d^2)/2b_r^2}\mathcal{J}_l(rd/b_r^2), \tag{2·3}$$

$$b_r=\sqrt{(4+x)/4x}\,b\,, \qquad b=\sqrt{\hbar\Omega/M_N}\,, \tag{2·4}$$

where $\phi_\alpha(\phi_x)$ represents the internal wf of $\alpha(x)$ cluster with ho $(0s)^4$ $((0s)^x)$ configuration in which the same size parameter $b=1.358$ fm is used for nucleons in the two clusters. The operator $\mathcal{A}'$ in Eq. (2·2) antisymmetrizes the nucleons belonging to different clusters. The generator coordinate d in the wave packet $\psi_l(r; d)$ specifies the α-x distance, and the $\mathcal{J}_l(z)$ in Eq. (2·3) is the spherical Bessel function with an imaginary argument. Here the size parameter b_r for the relative coordinate r is chosen to give the same ho frequency Ω as that for nucleons (Eq. (2·4)). In the same way, b_R entering into ho wf $u_{K\lambda}(R)$ is chosen as

$$b_R=\sqrt{\{(4+x)M_N+M_\Lambda\}/(4+x)M_\Lambda}\,b\,. \tag{2·5}$$

The total Hamiltonian of the $\alpha+x+\Lambda$ system can be written as

$$\mathcal{H}=H^{\alpha x}+T_R+V_{\Lambda N}\,, \tag{2·6}$$

where $H^{\alpha x}$ represents the $(4+x)$-nucleon part, T_R the kinetic energy associated with the (αx)-Λ relative coordinate $\boldsymbol{R}$, $V_{\Lambda N}$ the sum of Λ-N interactions; $V_{\Lambda N}=\sum_i v_{\Lambda N}(1, i)$. Starting with the Schrödinger equation $\mathcal{H}\Psi_J=E_J\Psi_J$, we can obtain the channel-coupled

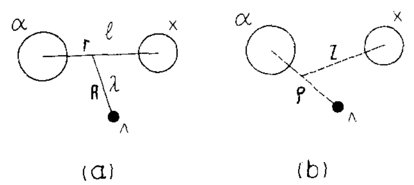

Fig. 1. (a). The coordinate system adopted to describe the three-cluster system ($x=n, p, d, t$ or α).
(b) The coordinate used in calculating the reduced width amplitude leading to the ${}^5_\Lambda$He-x decay channel.

seqular equation for the coefficient $w_c(d, K)$ of Ψ_J;

$$\sum_{c_2 d_2 K_2} \{\delta(l_1, l_2)\delta(K_1\lambda_1, K_2\lambda_2)\cdot \sum_{j_x j_\Lambda} \begin{bmatrix} l_1 & \lambda_1 & L_1 \\ S_x & S_\Lambda & S_1 \\ j_x & j_\Lambda & J \end{bmatrix} \begin{bmatrix} l_2 & \lambda_2 & L_2 \\ S_x & S_\Lambda & S_2 \\ j_x & j_\Lambda & J \end{bmatrix} H^{\alpha x}_{l_1 j_x}(d_1, d_2)$$

$$+\delta(c_1, c_2)\cdot T^R_{\lambda_1}(K_1, K_2) N^{\alpha x}_{l_1}(d_1, d_2) + \delta(L_1 S_1, L_2 S_2)\cdot U_J^{\Lambda N}(c_1 d_1 K_1, c_2 d_2 K_2)$$

$$-\delta(c_1, c_2)\delta(K_1\lambda_1, K_2\lambda_2)\cdot E_J N^{\alpha x}_{l_1}(d_1, d_2)\} w_{c_2}(d_2, K_2) = 0\,, \tag{2·7}$$

where definitions of the matrix elements are

$$\left.\begin{matrix} H^{\alpha x}_{lj}(d_1, d_2) \\ N_l^{\alpha x}(d_1, d_2) \end{matrix}\right\} = \langle [\Phi(l; d_1) S_x]; j | \left\{\begin{matrix} H^{\alpha x} \\ 1 \end{matrix}\right\} | [\Phi(l; d_2) S_x]; j \rangle, \tag{2·8}$$

$$T_\lambda{}^R(K_1, K_2) = \langle u_{K_1\lambda}(\boldsymbol{R}) | T_R | u_{K_2\lambda}(\boldsymbol{R}) \rangle \tag{2·9}$$

and

$$U_J{}^{\Lambda N}(c_1 d_1 K_1, c_2 d_2 K_2)$$
$$= \langle [\Phi(l_1; d_1) \times u_{K_1\lambda_1}(\boldsymbol{R})]_{L_1} [S_x S_\Lambda]_{S_1}; J | V_{\Lambda N} | [\Phi(l_2; d_2) \times u_{K_2\lambda_2}(\boldsymbol{R})]_{L_2} [S_x S_\Lambda]_{S_2}; J \rangle. \tag{2·10}$$

Here $H^{\alpha x}_{lj}(d_1, d_2)$ and $N_l{}^{\alpha x}(d_1, d_2)$ are the energy and normalization kernels in the generator coordinate method(GCM).[34] In Eq. (2·7) the total orbital angular momentum L and spin S of the $\alpha + x + \Lambda$ system are not individually conserved due to the presence of the spin-orbit potential in $H^{\alpha x}$, while $\boldsymbol{j}_x = \boldsymbol{l} + \boldsymbol{S}_x$ and $\boldsymbol{j}_\Lambda = \boldsymbol{\lambda} + \boldsymbol{S}_\Lambda$ are also not conserved due to the Λ-N spin-spin interaction. The L-S coupling description for Ψ_J, Eq. (2·1), can be readily transformed into the j_x-j_Λ coupling one. Both descriptions will be used according to the convenience of the physical understandings.

The motion of the Λ particle is determined by a sort of the folding potential $U_J{}^{\Lambda N}$ of Eq. (2·10) supplied by the $\alpha + x$ core nucleus. On the other hand, the Λ particle plays a glue-like role to give additional couplings between α and x clusters through the Λ-N interaction matrix element $U_J{}^{\Lambda N}$. The explicit expression of $U_J{}^{\Lambda N}(c_1 d_1 K_1, c_2 d_2 K_2)$ for the Gaussian type of Λ-N interaction is given in the Appendix.

2.2. *Orthogonality condition model for the α-x part*

For the α-x part we employ the orthogonality condition model (OCM)[35] instead of directly solving the GCM equation. The OCM has been proved to be a good approximation of GCM and also has an advantage of allowing the adjustment to reproduce the observed low-lying properties of the $\alpha + x$ core nucleus. By the OCM approximation we can take into account the essential effect of the Pauli principle arising from the nucleon antisymmetrization. In general the GCM basis function $\Phi(l; d)$ of Eq. (2·2) can be expanded in terms of the normalized-antisymmetrized ho basis functions $\{\widehat{\Phi}^{\alpha x}(Nl)\}$ of the α-x system:

$$\Phi(l; d) = \sum_N \sqrt{\mu_N} C_{Nl}(d; b_r) \widehat{\Phi}^{\alpha x}(Nl), \tag{2·11}$$

$$\widehat{\Phi}^{\alpha x}(Nl) = \frac{1}{\sqrt{1+\delta_{\alpha x}}} \sqrt{\frac{4!x!}{(4+x)!}} \frac{1}{\sqrt{\mu_N}} \mathcal{A}' \{\phi_\alpha \phi_x u_{Nl}(\boldsymbol{r})\}, \quad u_{Nl}(\boldsymbol{r}) = u_{Nl}(r) Y_l(\hat{\boldsymbol{r}}), \tag{2·12}$$

where $u_{Nl}(r)$ is the ho wf with the size b_r and quanta $N=2n+l$, and

$$C_{Nl}(d;\, b_r)=4\pi(-)^n\pi^{-1/4}2^{-3/2}[\Gamma(n+l+\frac{3}{2})\Gamma(n+1)]^{-1/2}(d/2b_r)^N e^{-(d/2b_r)^2}. \tag{2·13}$$

The coefficient μ_N is the eigenvalue of the normalization kernel defined by

$$\frac{1}{1+\delta_{ax}}\langle\phi_a\phi_x|\mathcal{A}'\{\phi_a\phi_x u_{Nl}(\boldsymbol{r})\}\rangle=\mu_N u_{Nl}(\boldsymbol{r}), \tag{2·14}$$

and is obtained as

$$\mu_N=\frac{1}{1+\delta_{ax}}\sum_{m=0}^{x}\frac{x!}{(x-m)!m!}(-)^m\left(1-\frac{4+x}{4x}m\right)^N. \tag{2·15}$$

The GCM normalization kernel is expressed by the expansion:

$$N_l^{ax}(d_1,\, d_2)=\sum_N \mu_N C_{Nl}(d_1;\, b_r)C_{Nl}(d_2;\, b_r). \tag{2·16}$$

For the GCM energy kernel we make the OCM approximation, which amounts to using $\langle[u_{N_1l}S_x];\, j|H^{ax}_{\rm OCM}|[u_{N_2l}S_x];\, j\rangle$ in place of $\langle\hat{\Phi}^{ax}(N_1l)S_x];\, j|H^{ax}|\hat{\Phi}^{ax}(N_2l)S_x];\, j\rangle$ to give

$$H^{ax}_{lj}(d_1,\, d_2)=\sum_{N_1N_2}\sqrt{\mu_{N_1}\mu_{N_2}}\,C_{N_1l}(d_1,\, b_r)C_{N_2l}(d_2,\, d_r)\langle[u_{N_1l}S_x];\, j|H^{ax}_{\rm OCM}|[u_{N_2l}S_x];\, j\rangle. \tag{2·17}$$

Here the OCM effective Hamiltonian $H^{ax}_{\rm OCM}$ consists of the relative kinetic energy, central, spin-orbit and Coulomb potentials between the a and x clusters,

$$H^{ax}_{\rm OCM}=T_r+V_c(\boldsymbol{r})+V_{\rm LS}(\boldsymbol{r})+V_{\rm Coul}(\boldsymbol{r}). \tag{2·18}$$

For $V_c(\boldsymbol{r})$ and $V_{\rm LS}(\boldsymbol{r})$ we employ the Gaussian type effective potentials,

$$V_c(\boldsymbol{r})=V_c{}^0 e^{-(r/\beta_c)^2}, \tag{2·19}$$

$$V_{\rm LS}(\boldsymbol{r})=V^0_{\rm LS}e^{-(r/\beta_{\rm LS})^2}(\boldsymbol{l}\cdot\boldsymbol{s}), \tag{2·20}*)$$

which strengths and ranges are determined by readjusting the a-x folding potentials to reproduce the observed low-lying properties of the corresponding nucleus. The used parameters are summarized in Table II. The Coulomb folding potential is given by

$$V_{\rm Coul}(\boldsymbol{r})=\frac{Z_1Z_2e^2}{r^2}{\rm erf}\left(r\Big/\sqrt{2-\frac{4+x}{4x}}b\right), \tag{2·21}$$

Table II. Parameters of the central and spin-orbit effective nuclear potentials between the alpha and x clusters. The a-t and a-a strengths are from Ref. 37). $(a=1/\beta^2)$

a-x	$V_c{}^0$	$\beta_c(a_c)$	$V^0_{\rm LS}$	$\beta_{\rm LS}(a_{\rm LS})$
	MeV	fm	MeV	fm
a-$n(p)$	−43.0	2.236(0.20)	−27.5	2.375(0.18)
a-d	−74.0[a]	2.294(0.19)	−0.15[b]	4.082(0.06)
a-t	−86.2	2.500(0.16)	−3.0	1.890(0.28)
a-a	−106.2	2.236(0.20)	−	−

a) $V_c{}^0=-78.4$ MeV for the $l=2$ state.
b) For this strength see the footnote on page 193.

*) For the ^{6}Li case this form is modified as $V_{\rm LS}(r)=V^0_{\rm LS}r^2e^{-(r/\beta)^2}(\boldsymbol{l}\cdot\boldsymbol{s})$.

where $Z_1=2$ for α and Z_2 is the number of protons in the x cluster and $\mathrm{erf}(z)$ denotes the error function.

2.3. *The Λ-N interaction*

The two-body Λ-N interaction is simply chosen as a Gaussian form with the range $\beta_{\Lambda N}$ equivalent to the two-pion exchange Yukawa,

$$v_{\Lambda N}(r)=v^0_{\Lambda N}e^{-(r/\beta_{\Lambda N})^2}(1+\eta\boldsymbol{\sigma}_\Lambda\cdot\boldsymbol{\sigma}_N),$$

$$v_{\Lambda N}=-38.19\,\mathrm{MeV}\,,\quad \beta_{\Lambda N}=1.034\,\mathrm{fm}\,,\quad \eta=-0.1\,. \tag{2·22}$$

This strength $v^0_{\Lambda N}$ was determined so as to reproduce the experimental Λ-binding energy in ${}^5_\Lambda\mathrm{He}(B_\Lambda{}^{\mathrm{exp}}=3.12\,\mathrm{MeV})$[35] by using the Λ-α folding potential obtained with $\phi_\alpha(b=1.358$ fm).[24] The value of η is chosen by considering the suggestions in the literature.[5),14),35)] The LS interaction is not considered here because the Λ single particle spin-orbit potential has been found to be very weak.[1]

§ 3. Expressions of various physical quantities

For the calculation of various physical quantities, it is convenient to reexpress the wave function Ψ_J in terms of the α-x ho basis $\{\hat{\Phi}^{\alpha x}(Nl)\}$ given by Eq. (2·12):

$$\Psi_J=\sum_{cNK}A_c(N,K)|[\hat{\Phi}^{\alpha x}(Nl)\times u_{K\lambda}(\boldsymbol{R})]_L[S_xS_\Lambda]_S;J\rangle, \tag{3·1}$$

where the expansion coefficients A are related with the original w's by

$$A_c(N,K)=\sqrt{\mu_N}\sum_d C_{Nl}(d;b_r)w_c(d,K). \tag{3·2}$$

In the formulae given in the following two subsections, $\alpha(x)$ cluster is generally represented as the mass number $A_1(A_2)$ nucleus with $Z_1(Z_2)$ protons ($A_1=4$, $Z_1=2$, $A_2=x$).

3.1. *Electric quadrupole and dipole transition probabilities*

In case that the spatial wf within a cluster is symmetrical under any exchange of the constituent protons and neutrons, the electric quadrupole operator can be effectively expressed as ($e_\mathrm{p}=e$, $e_\mathrm{n}=0$):

$$\mathcal{M}(\mathrm{E2})=\sum_{\mathrm{protons}}e\hat{q}(\boldsymbol{r}_i)=\frac{Z_1e}{A_1}\sum_{i=1}^{A_1}\hat{q}(\boldsymbol{r}_i)+\frac{Z_2e}{A_2}\sum_{i=A_1+1}^{A_1+A_2}\hat{q}(\boldsymbol{r}_i)$$

$$=\mathcal{M}(\mathrm{E2})_\Lambda+\mathcal{M}(\mathrm{E2})_c+X\,, \tag{3·3a}$$

$$\mathcal{M}(\mathrm{E2})_\Lambda=(Z_1+Z_2)e\xi^2\hat{q}(\boldsymbol{R}), \tag{3·3b}$$

$$\mathcal{M}(\mathrm{E2})_c=\frac{Z_1A_2{}^2+Z_2A_1{}^2}{(A_1+A_2)^2}e\hat{q}(\boldsymbol{r})+e\hat{Q}^{(\mathrm{int})}_{A_1}+e\hat{Q}^{(\mathrm{int})}_{A_2}\,, \tag{3·3c}$$

where $\hat{q}(\boldsymbol{r})=r^2Y_2(\hat{\boldsymbol{r}})$ is the mass quadrupole operator and $\hat{Q}^{(\mathrm{int})}_A$ is the quadrupole operator for the internal coordinates of A-cluster. See Fig. 1(a) for the coordinates $\boldsymbol{R}$ and $\boldsymbol{r}$. The X term in Eq. (3·3a) contains a factor proportional to $\boldsymbol{R}\cdot\boldsymbol{r}$, which has no contribution within the model space we will adopt. The factor ξ in Eq. (3·3b) originates from the condition of the center-of-mass rest of the total three-cluster system (A_1+A_2

$+\Lambda$) and

$$\xi = M_\Lambda / \{(A_1+A_2)M_N + M_\Lambda\}. \tag{3·4}$$

Under a similar condition the electric dipole operator can be written as

$$\mathcal{M}(\mathrm{E1}) = \sum_{\text{protons}} e\hat{m}(\boldsymbol{r}_i) = \mathcal{M}(\mathrm{E1})_\Lambda + \mathcal{M}(\mathrm{E1})_c\,, \tag{3·5a}$$

$$\mathcal{M}(\mathrm{E1})_\Lambda = -(Z_1+Z_2)e\xi\hat{m}(\boldsymbol{R}), \tag{3·5b}$$

$$\mathcal{M}(\mathrm{E1})_c = -\frac{Z_1A_2 - Z_2A_1}{A_1+A_2} e\hat{m}(\boldsymbol{r}), \tag{3·5c}$$

where $\hat{m}(\boldsymbol{r}) = rY_1(\hat{\boldsymbol{r}})$ is the dipole operator. One can recognize from Eqs. (3·4) and (3·5b) that the Λ particle behaves in the E1 transition as if it carries an effective charge $\tilde{e}_\Lambda^{(\mathrm{E1})} = -(Z_1+Z_2)M_\Lambda e/\{(A_1+A_2)M_N+M_\Lambda\}$. This is caused by the recoil of the core nucleus and the situation is similar to the case of the neutron E1 effective charge $\tilde{e}_{\mathrm{n}}^{(\mathrm{E1})} = -Ze/A$. The $\mathcal{M}(\mathrm{E2})_\Lambda$ of Eq. (3·3b) is similarly interpreted. If both clusters have respectively the same numbers of protons and neutrons, then the core nucleus part $\mathcal{M}(\mathrm{E1})_c$ (Eq. (3·5c)) vanishes as a natural consequence.

The reduced E$\mathcal{L}$ ($\mathcal{L}=2$ or 1) transition probability can be obtained in the standard way by using the initial and final state wf's expressed by Eq. (3·1):

$$B(E\mathcal{L}; J_i \to J_f) = \frac{1}{[J_i]} |\langle \Psi_{J_f} \| \mathcal{M}(\mathrm{E}\mathcal{L}) \| \Psi_{J_i} \rangle|^2\,, \quad [J] \equiv 2J+1\,, \tag{3·6}$$

$$\begin{aligned} \langle \Psi_{J_f} \| \mathcal{M}(\mathrm{E}\mathcal{L}) \| \Psi_{J_i} \rangle = &\sum_{c_f N_f K_f} \sum_{c_i N_i K_i} A_{c_f}(N_f, K_f) A_{c_i}(N_i, K_i) \sqrt{[J_f][J_i][L_f][L_i]} \\ &\times W(L_f S_f \mathcal{L} J_i; J_f L_i) \{ \delta(N_f l_f, N_i l_i) \cdot W(l_i \lambda_i L_f \mathcal{L}; L_i \lambda_f) \\ &\qquad \times \langle u_{K_f \lambda_f}(\boldsymbol{R}) \| \mathcal{M}(\mathrm{E}\mathcal{L})_\Lambda \| u_{K_i \lambda_i}(\boldsymbol{R}) \rangle \\ &+ \delta(K_f \lambda_f, K_i \lambda_i) \cdot W(l_f \lambda_f \mathcal{L} L_i; L_f l_i) \langle \hat{\Phi}^{\alpha x}(N_f l_f) \| \mathcal{M}(\mathrm{E}\mathcal{L})_c \| \hat{\Phi}^{\alpha x}(N_i l_i) \rangle \}. \end{aligned} \tag{3·7}$$

In the evaluation of the matrix element $\langle \mathcal{M}(E\mathcal{L}=2)_c \rangle$ between the di-cluster ho basis given by Eq. (2·12), some complications arise because the operator $\mathcal{M}(\mathrm{E2})_c$ (Eq. (3·3c)) contains $\hat{Q}^{(\mathrm{int})}$ and because the relative part is not always symmetrical under exchange of the nucleons belonging to different clusters. If we assume that the relative part is symmetrical; the assumption is exactly valid for the ${}^9_\Lambda\mathrm{Be} = \alpha+\alpha+\Lambda$ and ${}^6_\Lambda\mathrm{Li} = \alpha+d+\Lambda$ cases ($Z_1 = A_1/2$, $Z_2 = A_2/2$), we can evaluate the matrix element by dropping the antisymmetrizer $4!x!/(4+x)! \cdot \mathcal{A}'$ in the $\hat{\Phi}^{\alpha x}$ having larger ho quanta. Then we obtain, for $N_f > N_i$,

$$\begin{aligned} &\langle \hat{\Phi}^{\alpha x}(N_f l_f) \| \mathcal{M}(\mathrm{E2})_c \| \hat{\Phi}^{\alpha x}(N_i l_i) \rangle \\ &= \frac{1}{1+\delta_{\alpha x}} \frac{1}{\sqrt{\mu_{N_f}\mu_{N_i}}} \langle \phi_\alpha \phi_x u_{N_f l_f}(\boldsymbol{r}) \| \mathcal{M}(\mathrm{E2})_c \| \mathcal{A}' \{ \phi_\alpha \phi_x \phi_{N_i l_i}(\boldsymbol{r}) \} \rangle \end{aligned} \tag{3·8a}$$

$$= \sqrt{\frac{\mu_{N_i}}{\mu_{N_f}}} \frac{Z_1 A_2^2 + Z_2 A_1^2}{(A_1+A_2)^2} \langle u_{N_f l_f}(\boldsymbol{r}) \| e\hat{q}(\boldsymbol{r}) \| u_{N_i l_i}(\boldsymbol{r}) \rangle, \tag{3·8b}$$

where $\mathcal{M}(\mathrm{E2})_c$ is operated on the left side, by lowering its ho quanta, to get non-vanishing matrix element. In this procedure the internal quanta of α and x clusters cannot be lowered any more, hence $\hat{Q}^{(\mathrm{int})}\phi_{\alpha(x)}=0$ holds and only the relative part of $\mathcal{M}(\mathrm{E2})_c$ remains as in Eq. (3·8b), where Eq. (2·14) has been used.

3.2. *Magnetic dipole transitions and moments*

The magnetic dipole operator consists of the orbital and spin parts:

$$\mathcal{M}(\mathrm{M1})=\sum_i\sqrt{\frac{3}{4\pi}}\mu_i=\sum_i\sqrt{\frac{3}{4\pi}}(g_l^{(i)}\boldsymbol{l}_i+g_s^{(i)}\boldsymbol{s}_i), \tag{3·9}$$

where the sum runs over all the constituent particles and g's are relevant g-factors. The standard (bare) values of g-factors are employed here:

$$g_l^{(i)}=\begin{cases}1 & \mathrm{nm}\\ 0 & \\ 0 & \end{cases}, \quad g_s^{(i)}=\begin{cases}5.586 & \mathrm{nm} \quad (i=p)\\ -3.826 & \quad (\;\; n)\\ -1.228 & \quad (\;\; \Lambda)\end{cases}. \tag{3·10}$$

The spin part is easy to handle with and especialy its matrix element for the spin$=0$ cluster (α) vanishes.

The orbital part should be expressed in terms of relative and internal coordinates of the clusters. Under the condition that the spatial wf of a cluster is symmetric for the constituent protons and neutrons, we can rewrite the operator by using the relative $\boldsymbol{l}$ and $\boldsymbol{\lambda}$ and the internal $\bar{\boldsymbol{L}}_{A_1}^{(\mathrm{int})}$ and $\bar{\boldsymbol{L}}_{A_2}^{(\mathrm{int})}$;

$$\begin{aligned}\sum_{i=1}^{A_1+A_2+\Lambda} g_l^{(i)}\boldsymbol{l}_i &= \frac{Z_1g_l^{(p)}+N_1g_l^{(n)}}{A_1}\sum_{i=1}^{A_1}(\boldsymbol{r}_i\times\boldsymbol{p}_i)+\frac{Z_2g_l^{(p)}+N_2g_l^{(n)}}{A_2}\sum_{i=A_1+1}^{A_1+A_2}(\boldsymbol{r}_i\times\boldsymbol{p}_i)\\ &\quad +g_l^{(\Lambda)}(\boldsymbol{r}_\Lambda\times\boldsymbol{p}_\Lambda)\\ &=\frac{Z_1A_2^2+Z_2A_1^2}{A_1A_2(A_1+A_2)}\boldsymbol{l}+\frac{Z_1g_l^{(p)}}{A_1}\bar{\boldsymbol{L}}_{A_1}^{(\mathrm{int})}+\frac{Z_2g_l^{(p)}}{A_2}\bar{\boldsymbol{L}}_{A_2}^{(\mathrm{int})}+\frac{Z_1+Z_2}{A_1+A_2}\xi\boldsymbol{\lambda}+Y,\end{aligned} \tag{3·11}$$

where the Y term contains the mixed products of the coordinate and non-conjugate momentum such as $\boldsymbol{R}\times\boldsymbol{p}_r$ and $\boldsymbol{r}\times\boldsymbol{p}_R$, and this doubly partity-changing term is inactive within the model space adopted in the present calculation. Furthermore, the two $\bar{\boldsymbol{L}}^{(\mathrm{int})}$-terms have no contribution for the s-shell clusters as in the present case.

From the above consideration we regard that the operator $\mathcal{M}(\mathrm{M1})$ for the $\alpha+x+\Lambda$ system consists of four effective parts: $\mathcal{M}(\mathrm{M1})_l^{\alpha x}$, $\mathcal{M}(\mathrm{M1})_\lambda^{\Lambda}$, $\mathcal{M}(\mathrm{M1})_s^{\alpha x}$ and $\mathcal{M}(\mathrm{M1})_s^{\Lambda}$ for which the notations should be self-evident. Then the reduced M1 transition probability and moment are given by

$$B(\mathrm{M1}; J_i\to J_f)=\frac{1}{[J_i]}|\langle\Psi_{J_f}\|\mathcal{M}(\mathrm{M1})\|\Psi_{J_i}\rangle|^2, \tag{3·12}$$

$$\mu(J)=\sqrt{\frac{4\pi}{3}}\frac{\langle JJ10|JJ\rangle}{[J]}\langle\Psi_J\|\mathcal{M}(\mathrm{M1})\|\Psi_J\rangle, \tag{3·13}$$

$$\begin{aligned}\langle\Psi_{J_f}\|\mathcal{M}(\mathrm{M1})\|\Psi_{J_i}\rangle &= \sum_{c_fN_fK_f}\sum_{c_iN_iK_i}A_{c_f}(N_f, K_f)A_{c_i}(N_i, K_i)\sqrt{[J_f][J_i]}\\ &\quad\times[\delta(S_f, S_i)\cdot\sqrt{[L_f][L_i]}\,W(L_fS_f1J_i; J_fL_i)\\ &\quad\times\{\delta(K_f\lambda_f, K_i\lambda_i)\cdot W(l_f\lambda_f1L_i; L_fl_i)\langle\hat{\Phi}^{\alpha x}(N_fl_f)\|\mathcal{M}(\mathrm{M1})_l^{\alpha x}\|\hat{\Phi}^{\alpha x}(N_il_i)\rangle\end{aligned}$$

$$+\delta(N_fl_f,\,N_il_i)\cdot W(l_i\lambda_iL_f1;\,L_i\lambda_f)\langle u_{K_f\lambda_f}(\boldsymbol{R})\|\mathcal{M}(\mathrm{M1})_\lambda{}^{\Lambda}\|u_{K_i\lambda_i}(\boldsymbol{R})\rangle\}$$
$$+\delta(N_fl_f,\,N_il_i)\delta(K_f\lambda_f,\,K_i\lambda_i)\cdot\delta(L_f,\,L_i)\cdot\sqrt{[S_f][S_i]}\,W(L_iS_iJ_f1;\,J_iS_f)$$
$$\times\{W(S_xS_\Lambda 1S_i;\,S_fS_x)\langle S_x\|\mathcal{M}(\mathrm{M1})_s{}^{\alpha x}\|S_x\rangle$$
$$+W(S_xS_\Lambda S_f1;\,S_iS_\Lambda)\langle S_\Lambda\|\mathcal{M}(\mathrm{M1})_s{}^{\Lambda}\|S_S\rangle\}]. \tag{3·14}$$

The same procedure as used to obtain Eq. (3·3b) is applied here and

$$\langle\hat{\Phi}^{\alpha x}(N_fl_f)\|\mathcal{M}(\mathrm{M1})_l{}^{\alpha x}\|\hat{\Phi}^{\alpha x}(N_il_i)\rangle$$
$$=\delta(N_fl_f,\,N_il_i)\sqrt{\frac{3}{4\pi}\frac{Z_1A_2{}^2+Z_2A_1{}^2}{A_1A_2(A_1+A_2)}}\sqrt{l_i(l_i+1)(2l_i+1)}\,, \tag{3·15}$$

$$\langle u_{K_f\lambda_f}(\boldsymbol{R})\|\mathcal{M}(\mathrm{M1})_\lambda{}^{\Lambda}\|u_{K_i\lambda_i}(\boldsymbol{R})\rangle=\delta(K_f\lambda_f,\,K_i\lambda_i)\sqrt{\frac{3}{4\pi}}\frac{Z_1+Z_2}{A_1+A_2}\xi\sqrt{\lambda_i(\lambda_i+1)(2\lambda_i+1)}\,, \tag{3·16}$$

$$\langle S_x\|\mathcal{M}(\mathrm{M1})_s{}^{\alpha x}\|S_x\rangle$$
$$=\sqrt{\frac{3}{4\pi}}\sqrt{\frac{3}{2}}\times\begin{cases} g_s{}^{(x)} & (x=n \text{ or } p)\\ g_s{}^{(n)}+g_s{}^{(p)} & (x=d)\\ \{g_s{}^{(n)}+g_s{}^{(p)}+(g_s{}^{(n)}-g_s{}^{(p)})T_z\}/2 & (x=t;\ T_z=1/2)\\ 0 & (x=\alpha)\end{cases} \tag{3·17}$$

$$\langle S_\Lambda\|\mathcal{M}(\mathrm{M1})_s{}^{\Lambda}\|S_\Lambda\rangle=\sqrt{\frac{3}{4\pi}}\sqrt{\frac{3}{2}}g_s{}^{(\Lambda)} \qquad \text{with } A_1=4,\ Z_1=2,\ A_2=x\,. \tag{3·18}$$

3.3. *Reduced width amplitudes and spectroscopic factors*

Another important quantity is the reduced width amplitudes (RWA) leading to the i) (αx)-Λ and ii) ${}^5_\Lambda$He-x channels. The fomer corresponds to the separation process and the latter the break-up into the two clusters.

—— (αx)-Λ channel ——

The RWA for the (αx)-Λ channel is defined and expressed by

$$\mathcal{Y}^{\alpha x\text{-}\Lambda}_{lj_x\text{-}\lambda j_\Lambda}(R)\equiv R\langle[\mathring{\Phi}_{jx}(l)S_x]_{j_x}[Y_\lambda(\hat{\boldsymbol{R}})S_\Lambda]_{j_\Lambda};J|\Psi_J\rangle \tag{3·19}$$

$$=\sum_N a_N{}^{(lj_x)}\sum_{LSK}\begin{bmatrix} l & S_x & j_x\\ \lambda & S_\lambda & j_\Lambda\\ L & S & J\end{bmatrix}A_c(N,\,K)u_{K\lambda}(R), \tag{3·20}$$

where the square bracket is the normalized 9-j symbol and $A_c(N,\,K)$ is given by Eq. (3·2). Recall that $u_{K\lambda}(R)$ is the ho wf with the size parameter b_R. The $a_N{}^{(lj_x)}$'s are the expansion coefficients of the free α-x wf $|\mathring{\Phi}_{jx}(l)S_x;\,j_x\rangle$ with respect to the normalized-antisymmetrized ho basis $\{|\hat{\Phi}^{\alpha x}(Nl)S_x;\,j_x\rangle\}$ defined by Eq. (2·12). The coefficients are related with the α-x GCM amplitudes $f_{lj_x}(d)$ by

$$|\mathring{\Phi}_{jx}(l)S_x;\,j_x\rangle=\sum_d f_{lj_x}(d)|\Phi(l;\,d)S_x;\,j_x\rangle=\sum_N a_N{}^{(lj_x)}|\hat{\Phi}^{\alpha x}(Nl)S_x;\,j_x\rangle, \tag{3·21}$$

$$a_N^{(ljx)}=\sqrt{\mu_N}\sum_d f_{ljx}(d)C_{Nl}(d;\,b_r\,). \tag{3·22}$$

Table III lists the coefficients $a_N^{(ljx)}$. The corresponding spectroscopic factor $S^2_{lj_x\text{-}\lambda j_\Lambda}$ is defined by the norm of the RWA,

$$S^2_{lj_x\text{-}\lambda j_\Lambda}=\int_0^\infty [\mathcal{Y}^{\alpha x\text{-}\Lambda}_{lj_x\text{-}\lambda j_\Lambda}(R)]^2dR\,. \tag{3·23}$$

The RWA and S^2 in the shell-model limit are obtained in our model by putting

$$a_N^{(ljx)}=\delta(N,\,N_0), \tag{3·24a}$$

$$A_c(N,\,K)=\begin{cases}\text{normalized to 1 within the } N=N_0 \text{ and } K=K_0 \text{ space}\\ 0 \qquad \text{for } N>N_0 \text{ or } K>K_0\,,\end{cases} \tag{3·24b}$$

where $N_0(K_0)$ is the lowest allowed quanta for the α-x $((\alpha x)$-$\Lambda)$ relative motion, i.e., $N_0=x$ and $K_0=0(1)$ for the normal (non-normal) parity state.

Table III. Harmonic oscillator expansion coefficients $a_N^{(lj)}$ of the "α-x" ground state wave functions. See Eqs. (3·21) and (3·22) for the definition and Eq. (2·12) for the di-cluster ho basis. They are normalized as $\sum_N|a_N|^2=1$. The ho expansion coefficients a of the ${}^5_\Lambda$He$(1/2^+)$ ground state wf are also listed on the right side (see Eq. (3·27)). Note that $N=2n+l$.

$l(j^\pi)$	α-$n(p)$ $1(3/2^-)$	α-d $0(1^+)$	α-t $1(3/2^-)$	α-α $0(0^+)$	α-Λ $0(1/2^+)$
$n=0$	0.799	*	*	*	0.922
1	−0.369	−0.743	0.741	*	−0.251
2	0.317	0.420	−0.459	0.569	0.229
3	−0.230	−0.335	0.336	−0.448	−0.127
4	0.185	0.252	−0.242	0.394	0.101
5	−0.148	−0.192	0.174	−0.332	−0.066
6	0.105	0.152	−0.128	0.274	0.049
7	−0.064	−0.124	0.097	−0.225	−0.032
8	0.035	0.099	−0.074	0.182	0.020
⋮	⋮	⋮	⋮	⋮	⋮

* Forbidden states.

—— *${}^5_\Lambda$He-x channel* ——

By choosing the inter-cluster Jacobi coordinates ρ and Z illustrated in Fig. 1(b), the RWA for the ${}^5_\Lambda$He$(1/2^+_g)$-x channel is defined by

$$\mathcal{Y}^{\alpha\Lambda\text{-}x}_{LJ_x}(Z)=\frac{1}{\sqrt{1+\delta_{\alpha x}}}\sqrt{\frac{(4+x)!}{4!x!}}\,Z\,\langle\phi[{}^5_\Lambda\text{He}(1/2^+)][\phi_x Y_L(\hat{\boldsymbol{Z}})S_x]_{J_x};\,J|\Psi_J\rangle, \tag{3·25}$$

where the ground state wf of ${}^5_\Lambda$He is given by the s-state α-Λ wf $\xi_0(\rho)$ as

$$\phi[{}^5_\Lambda\text{He}(1/2^+)]=\phi_\alpha\xi_0(\rho)[Y_0(\hat{\boldsymbol{\rho}})S_\Lambda]_{1/2}\,. \tag{3·26}$$

We expand the $\xi_0(\rho)$ in terms of the ho wf $u_{N0}(\rho;\,b_\rho)$ with the appropriate size parameter b_ρ which assures the common oscillator constant $(\mu_\rho b_\rho^{\,2}=M_N b^2=\hbar/\Omega)$;

$$\xi_0(\rho)=\sum_N\tilde{a}_N u_{N0}(\rho;\,b_\rho),\quad b_\rho=\sqrt{(4M_N+M_\Lambda)/4M_\Lambda}\,b\,. \tag{3·27}$$

The coefficients $\tilde{a}_N$ are listed in the 6th column of Table III. Note that they are obtained by solving the Λ-α problem with the Λ-N interaction described in § 2.3. By using Eqs. (3·26) and (3·27) along with the j-j to L-S recoupling, we obtain final expression of the RWA:

$$\mathcal{Y}^{\alpha\Lambda\text{-}x}_{LJx}(Z)=\sum_{N'}\tilde{a}_{N'}\sum_{l\lambda S}(-)^{S_x+S_\Lambda-S}\begin{bmatrix} 0 & S_\Lambda & 1/2 \\ L & S_x & J_x \\ L & S & J \end{bmatrix}$$

$$\times\sum_{NK}\sqrt{\mu_N}A_c(N,K)\langle N'0(\boldsymbol{\rho}),K'L(\boldsymbol{Z})|Nl(\boldsymbol{r}),K\lambda(\boldsymbol{R})\rangle_L u_{K'L}(Z;b_Z), \tag{3·28a}$$

$$K'=N+K-N', \qquad b_Z=\sqrt{\frac{(4+x)M_N+M_\Lambda}{x(4M_N+M_\Lambda)}}\,b, \tag{3·28b}$$

where $\langle|\rangle_L$ indicates the ho Moshinsky bracket between different Jacobi coordinates for three particles (Fig. 1(a) vs (b)), and $u_{K'L}(Z;b_Z)$ is the ho wf relevant to the ${}^5_\Lambda$He-x relative coordinate Z. The corresponding spectroscopic factor is similarly given by

$$S^2_{LJx}=\int_0^\infty[\mathcal{Y}^{\alpha\Lambda\text{-}x}_{LJx}(Z)]^2dZ. \tag{3·29}$$

The shell-model limit values of the RWA and S-factor are obtained by setting $\tilde{a}_{N'}=\delta(N',0)$ together with a condition similar to Eq. (3·24b).

On the basis of the separation energy method,[38),39)] the partial decay widths of the resonance levels are estimated from the relevant RWA:

$$\Gamma_L=2P_L(a)\gamma_L{}^2(a), \tag{3·30}$$

$$\gamma_L{}^2(a)=\theta_L{}^2(a)\gamma_W{}^2(a), \qquad \gamma_W{}^2(a)=\frac{3\hbar^2}{2\mu a^2}, \tag{3·31a}$$

$$\theta_L{}^2(a)=\frac{a}{3}\mathcal{Y}_L{}^2(a), \tag{3·31b}$$

where the penetration factor P_L, the reduced width $\theta_L{}^2$ and the Wigner limit $\gamma_W{}^2$ are evaluated at an appropriate channel radius a.

3.4. *Effective neutron numbers for* (K^-,π^-) *reactions*

The (K^-,π^-) reaction experiments have been arranged so that the momentum transfer to the produced hyperon becomes very small and the recoilless Λ-production can take place in nuclei.[1),5)] Informations of the hypernuclear structure can be deduced by using the distorted wave impulse approximation (DWIA), in which the (K^-,π^-) reaction cross section is related to the elementary $K^-n\to\Lambda\pi^-$ cross section by[12),14),40),41)]

$$\left.\frac{d\sigma_{if}(\theta)}{d\Omega}\right|^{\rm lab}=N_{\rm eff}(i\to f;\theta)\left.\frac{d\sigma(\theta)}{d\Omega}\right|^{\rm lab}_{K^-n\to\Lambda\pi^-}. \tag{3·32}$$

The effective neutron number $N_{\rm eff}(i\to f;\theta)$ is given by

$$N_{\rm eff}(i\to f;\theta)=\frac{1}{[J_i]}\sum_{M_fM_i}\left|\langle f|\int d^3\boldsymbol{r}\,\chi^{(-)*}_{p_\pi}(\boldsymbol{r})\chi^{(+)}_{p_K}(\boldsymbol{r})\sum_{k=1}^{A}U_-(k)\delta(\boldsymbol{r}-\boldsymbol{r}_k)|i\rangle\right|^2, \tag{3·33a}$$

$$=\frac{4\pi}{[J_i]}\sum_{\kappa\mu}|\langle J_f T_f \tau_f \| \sum_k U_-(k)\tilde{j}_{\kappa\mu}(\theta; r_k) Y_\kappa(\hat{\boldsymbol{r}}_k) \| J_i T_i \tau_i \rangle|^2 . \quad (3\cdot33\text{b})$$

Here the U-spin lowering operator U_- transforms a neutron into a Λ-particle. The expression Eq. (3·33b) is obtained by making a partial wave expansion of the distorted waves of the K^- and π^- mesons,

$$\chi_{p_\pi}^{(-)*}(\boldsymbol{r})\chi_{p_K}^{(+)}(\boldsymbol{r})=\sum_{\kappa\mu}\sqrt{4\pi[\kappa]}\, i^\kappa \tilde{j}_{\kappa\mu}(\theta; r) Y_{\kappa\mu}(\hat{\boldsymbol{r}}), \quad (3\cdot34)$$

where K^- beam direction is chosen as the z-axis. The function $\tilde{j}_{\kappa\mu}(\theta; r)$ which depends implicitly on the momenta p_K and p_π is calculated by employing the eikonal approximation with pure imaginary optical potentials proportional to nuclear density.

Now we derive the expression of N_{eff} for the reaction $[\alpha+(x+1)](K^-, \pi^-)[\alpha+x+\Lambda]$ on the basis of our microscopic cluster model. As for the ground state of ^{9}Be ($x=4$ target nucleus), we use the wf calculated by Okabe et al.[42] in the framework of the microscopic $\alpha+\alpha+n$ three-cluster model. The ground state wf's of the target nuclei with $x\leqq3$ are obtained by solving the $\alpha+x_1$ two-cluster problem ($x_1=x+1$) and are given in terms of the ho basis (Eq. (2·12)) by

$$\Psi_{J_i T_i \tau_i}^{\alpha x_1}=\sum_{N_i} a_{N_i}^{(L_i J_i)} |\hat{\Phi}_{T_i \tau_i}^{\alpha x_1}(N_i L_i) S_i; J_i\rangle . \quad (3\cdot35)$$

With the aid of the overlap relation corresponding to the change of Jacobi coordinates, i.e.,

$$\sqrt{5+x}\langle[\hat{\Phi}_{T_f\tau_f}^{\alpha x}(N'l')Y_{\lambda_i}(\hat{\boldsymbol{R}})]_{L_i}[S_x\times\tfrac{1}{2}]_{S_i}|\hat{\Phi}_{T_i\tau_i}^{\alpha x_1}(N_iL_i)S_i\rangle$$

$$=\omega_x(T_i\tau_iS_i;\ T_f\tau_fS_x)\Omega_x(N_iL_i;\ N'l',\ K_i\lambda_i)u_{K_i\lambda_i}(R)|\tfrac{1}{2},\ \tau_i-\tau_f\rangle, \quad (3\cdot36)$$

$$(K_i=N_i-N')$$

the $\alpha+(x+1)$ target wf in Eq. (3·33b) can be effectively expressed as

$$\Psi_{J_iT_i\tau_i}^{\alpha x_1}=\sum_{N_i}\sum_{N'l'K_i\lambda_i}\omega_x(T_i\tau_iS_i;\ T_f\tau_fS_x)\Omega_x(N_iL_i;\ N'l';\ N'l',\ K_i\lambda_i)$$

$$\times|[\hat{\Phi}_{T_f\tau_f}^{\alpha x}(N'l')\times u_{K_i\lambda_i}(\boldsymbol{R})]_{L_i}[S_x\times\tfrac{1}{2}]_{S_i};\ J_i\rangle . \quad (3\cdot37)$$

The coefficients ω_x and Ω_x are given as follows:

$$\omega_x(T_i\tau_iS_i;\ T_f\tau_fS_x)=\begin{cases} 1 & \text{for } x=1\ (^6\text{Li};\ ^6_\Lambda\text{Li}) \\ \sqrt{3/2} & \text{for } x=2\ (^7\text{Li};\ ^7_\Lambda\text{Li}) \\ 1 & \text{for } x=4\ (^9\text{Be};\ ^9_\Lambda\text{Be}), \end{cases} \quad (3\cdot38)$$

$$\Omega_x(N_iL_i;\ N'l',\ K_i\lambda_i)=\sqrt{5+x}\langle[\hat{\Phi}^{\alpha x}(N'l')\times u_{K_i\lambda_i}(\boldsymbol{R})]_{L_i}|\hat{\Phi}^{\alpha x_1}(N_iL_i)\rangle . \quad (3\cdot39)$$

Note that the wf of ^{9}Be target is provided in the form of $\alpha+\alpha+n$. Using the target nuclear wf, Eq. (3·35), and the final state hypernuclear wf given by Eq. (3·1), we can get the cluster-model expression for N_{eff}:

$$N_{\text{eff}}(J_iT_i\tau_i\to J_fT_f\tau_f;\theta)=\frac{1}{[J_i]}\omega_x(T_i\tau_iS_i;\ T_f\tau_fS_x)^2\sum_{\kappa\mu}|\mathcal{M}_{\kappa\mu}(J_i,\ J_f)|^2 , \quad (3\cdot40)$$

$$\mathcal{M}_{\kappa\mu}(J_i, J_f)=\sum_{C_fN_fK_f}\sum_{C_iN_iK_i} A_{C_f}(N_fK_f)a_{N_i}^{(L_iJ_i)}\delta(S_f, S_x)\sqrt{[J_f][J_i][L_f][L_i][\lambda_i][\varkappa]}$$

$$\times W(L_fS_f\varkappa J_i; J_fL_i)W(l_f\lambda_iL_f\varkappa; L_i\lambda_f)(\lambda_i0\varkappa0|\lambda_f0)\Omega(N_iL_i; N_fl_f, K_i\lambda_i)$$

$$\times\langle u_{K_f\lambda_f}(R)\|\tilde{j}_{\kappa\mu}\Big(\theta; \frac{4+x}{5+x}R\Big)\|u_{K_i\lambda_i}(R)\rangle, \quad K_i=N_i-N_f . \tag{3·41}$$

$$(N_i=2n_i+L_i,\ N_f=2n_f+l_f,\ K_i=2\nu_i+\lambda_i)$$

The (K^-, π^-) forward cross sections which have been observed most intensively concern the effective neutron number at $\theta=0°$. In the following we will calculate $N_{\rm eff}$ $(i\to f; \theta=0°)$ and also the total effective neutron number $N_{\rm eff}^{\rm tot}(\theta=0°)$ for reactions on ^{6}Li, ^{7}Li and ^{9}Be for which experimental data are available. The $N_{\rm eff}^{\rm tot}(\theta=0°)$ is defined by a sum of all final hypernuclear state contributions and simply expressed as

$$N_{\rm eff}^{\rm tot}(\theta=0°)=\int\rho_n(\boldsymbol{r})|\chi_{p_\pi}^{(-)*}(\boldsymbol{r})\chi_{p_K}^{(+)}(\boldsymbol{r})|^2d^3\boldsymbol{r}\,, \tag{3·42}$$

where $\rho_n(r)$ is the neutron density of the target nucleus and is calculated with our cluster model wf.

§ 4. Results and discussion

As mentioned in § 2.1, our model space is described by the channels of possible angular momentum couplings $c=\{l\lambda LS\}$, the α-x generator coordinate d and the (αx)-Λ harmonic oscillator (ho) quanta $K=2\nu+\lambda$. In the present calculation, the inter-cluster states are restricted to the following space:

(I) the α-x orbital $l=1$ and 3 for $^6_\Lambda$He, $^6_\Lambda$Li and $^8_\Lambda$Li; $l=0$ and 2(0,2 and 4) for $^7_\Lambda$Li ($^9_\Lambda$Be),

(II) the GCM mesh points: $d=1.0$, 2.25, 3.5, 5.0 and 6.5 fm,

(III) the (αx)-Λ ho quanta $K=2\nu+\lambda$ with $0\leqq\nu\leqq9$ and $0\leqq\lambda\leqq3$ (or 4).

Note that the description of low-lying properties of the $\alpha+x$ nuclear systems can be satisfactorily achieved within the model space of (I) and (II). Table III lists the ho expansion coefficients of the α-x nuclear ground state wave functions (wf). In the following we will discuss the calculated results on $^9_\Lambda$Be, $^8_\Lambda$Li, $^7_\Lambda$Li and $^6_\Lambda$He ($^6_\Lambda$Li) in this order.

4.1. *The hypernucleus* $^9_\Lambda$*Be*

The calculated energy spectra of $^9_\Lambda$Be and dominant components of their wf's are shown in Figs. 2 and 3 where the calculated ^{8}Be spectrum is also displayed. In this case with spin$=0$ $\alpha+\alpha$ core, the $\boldsymbol{\sigma}_\Lambda\cdot\boldsymbol{\sigma}_N$ part of the Λ-N interaction is inactive and each level is degenerate for the Λ-spin up and down. The spectrum can therefore be classified by the orbital angular momentum L instead of the total $J=L\pm1/2$. The positive parity states with $J^\pi=1/2^+(L^\pi=0^+)$, $3/2^+$-$5/2^+(2^+)$ and $7/2^+$-$9/2^+(4^+)$ constitute the ground rotational band (intrinsic orbital quantum number $K^\pi=0^+$) and 94.5% of their wf's is occupied by the s-state Λ-particle coupled to the ^{8}Be ground rotational members ($l=0$, 2, 4), respectively. In fact the $K=0^+$ spectrum just parallels that of ^{8}Be as seen in Fig. 3. It is interesting, however, to note that the α-α distance $\sqrt{\langle r^2\rangle_{\alpha\text{-}\alpha}}$ in $^9_\Lambda$Be is cosiderably contracted due to the attractive Λ-N interaction (see Table IV).

The negative parity states separate into two bands:

(i) $K^\pi=0^-$ band: $L=1^-$, 3^- and 5^- $(J=L\pm1/2)$,

(ii) $K^\pi=1^-$ band: $L=1^-$, 2^-, 3^- and 4^- $(J=L\pm1/2$, "^{9}Be-analog").

This two-band level structure is clearly exhibited in the wf components and is confirmed by the B(E2) relations shown in Fig. 3. This feature allows one to take the strong coupling picture. The large stable deformation due to the α-α clustering in $^9_\Lambda$Be enhances the realization of the picture.[31),43)]

We have three particle-stable bound states, $J=1/2^+$(g.s.), $3/2^+$-$5/2^+$(3.06 MeV), for $^9_\Lambda$Be in contrast to the ^{8}Be case. Note that the lowest threshold energy is 3.12 MeV for the $^5_\Lambda$He-α channel. The Λ-particle binding energy in the ground state of $^9_\Lambda$Be is obtained as $B_\Lambda=7.49$ MeV, which is a little overestimated in comparison with the observed $B_\Lambda^{\rm exp}=6.71$ MeV.[35)]

In order to study the level characteristics, reduced E2 transition probabilities are calculated between the obtained eigenstates even in the unbound energy region. In Fig. 3 the $B({\rm E2}; L\to L')$ values in unit of e^{2}fm^4 are shown with arrows instead of $B({\rm E2}; J\to J')$ $=[L][J']W(L'\frac{1}{2}2J; J'L)^2B({\rm E2}; L\to L')$ for $J=L\pm1/2$. The strong intra-band and weak inter-band transition rates give another confirmation of the three-band level structure mentioned above. Reflecting the dynamical contraction of the α-α distance in $^9_\Lambda$Be (Table IV), the $4^+\to2^+\to0^+$ E2 transition probabilities become nearly half the corresponding cascades in ^{8}Be. It should be noted that the present B(E2) values in the $K=0^+$ band ($K=0^-$ and 1^- bands) are about 6(10) times larger than our shell-model limit values defined in § 3.3. This feature of B(E2) is similar to the first estimate in BSS.[31)] Our B(E2)

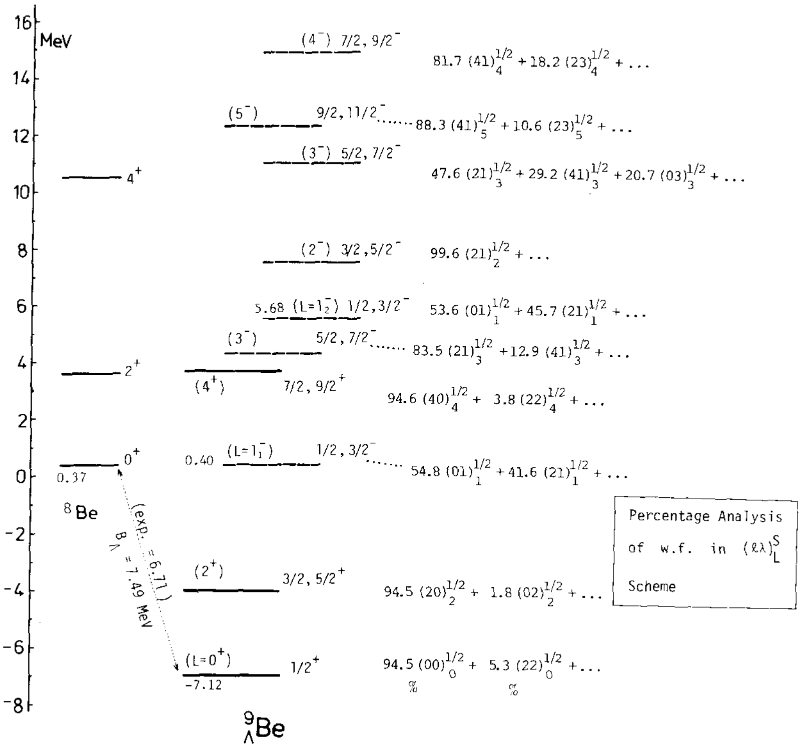

Fig. 2. Calculated energy spectra of ^{8}Be and $^9_\Lambda$Be. The energy scale is the relative binding energy among the constituent clusters. The dominant components of the L-S coupling $^9_\Lambda$Be wave functions are given in %.

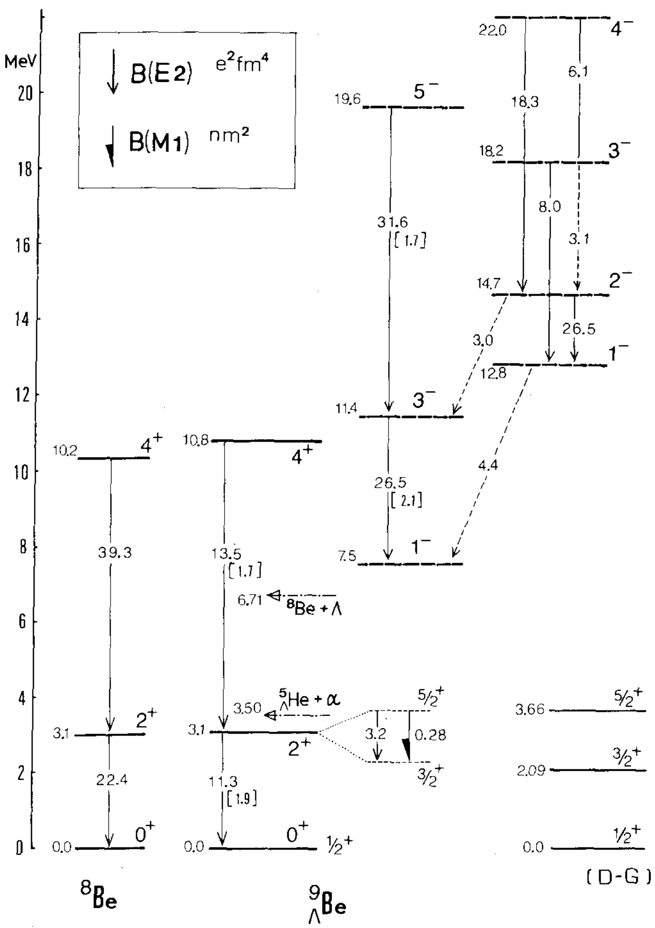

Fig. 3. Calculated reduced E2 and M1 transition probabilities in ^{8}Be and $^9_\Lambda$Be. The levels of $^9_\Lambda$Be are assigned orbital angular momentum L instead of the degenerate $J=L\pm 1/2$, hence the $B(\mathrm{E2}; L\rightarrow L')$ are listed in this figure except the case $5/2^+\rightarrow 3/2^+$. The B(E2) values less than the Weisskopf estimate ($1.1e^2\mathrm{fm}^4$) are not shown. In the square brackets are the shell-model limit values described in the text. The experimental threshold energies are indicated in the $^9_\Lambda$Be spectrum. The shell-model levels predicted by Dalitz and and Gal (D-G)[15] are compared.

Table IV. Root-mean-square estimates of the α-α and ^{8}Be-Λ distances in $^9_\Lambda$Be as compared with those of ^{8}Be. Note that $\sqrt{\langle r^2\rangle_\alpha}=1.44$ fm with $b=1.358$ fm. The root-mean-square radii of the total system are also listed.

^{8}Be			$^9_\Lambda$Be							(fm)
J	$\sqrt{\langle r^2\rangle_{\alpha\text{-}\alpha}}$	Tot	L	$\sqrt{\langle r^2\rangle_{\alpha\text{-}\alpha}}$	$\sqrt{\langle R^2\rangle_\Lambda}$	Tot	L	$\sqrt{\langle r^2\rangle_{\alpha\text{-}\alpha}}$	$\sqrt{\langle R^2\rangle_\Lambda}$	Tot
0^+	4.09	2.50	0^+	3.46	2.39	2.25	1^-	4.05	3.50	2.58
2^+	4.17	2.53	2^+	3.44	2.39	2.24	1^-	3.92	4.93	2.76
							2^-	3.95	4.94	2.77
							3^-	4.14	3.79	2.65
4^+	4.66	2.74	4^+	3.33	2.37	2.21	3^-	4.11	5.17	2.85
							4^-	4.25	5.29	2.93
							5^-	4.43	4.35	2.83

estimates are significantly larger than the shell-model predictions by Dalitz and Gal (D-G)[15] who obtained a large splitting between the first doublet; $3/2^+$ state at 2.09 MeV and $5/2^+$ state at 3.66 MeV above the ground $1/2^+$ state:

$$T(\mathrm{E2};\,3/2^+\to 1/2^+)=3.9\times10^{12}\,\mathrm{sec}^{-1};\quad B(\mathrm{E2})=11.26\,\mathrm{e}^2\mathrm{fm}^4\qquad (\text{D-G: }3.54\,\mathrm{e}^2\mathrm{fm}^4),$$
$$T(\mathrm{E2};\,5/2^+\to 1/2^+)=3.9\times10^{12}\,\mathrm{sec}^{-1};\quad B(\mathrm{E2})=11.26\,\mathrm{e}^2\mathrm{fm}^4\qquad (\text{D-G: }3.49\,\mathrm{e}^2\mathrm{fm}^4),$$
$$B(\mathrm{E2};\,5/2^+\to 3/2^+)=3.24\,\mathrm{e}^2\mathrm{fm}^4\,.$$

The non-vanishing M1 cascades within the $K=0^+$ band exists for the spin-flip transitions of $5/2^+\to3/2^+$ and $9/2^+\to7/2^+$, though the doublets are respectively degenerate in our model:

$$B(\mathrm{M1};\,5/2^+\to3/2^+)=0.28\,\mathrm{nm}^2\qquad(\text{D-G}: 0.32\,\mathrm{nm}^2),$$
$$B(\mathrm{M1};\,9/2^+\to7/2^+)=0.31\,\mathrm{nm}^2.$$

The predicted lifetime of the first excited state is now

$$\tau(3/2^+)=0.27\,\mathrm{psec}\ [1.61\,\mathrm{psec}]\qquad(\text{D-G}: 1.43\sim5.81\,\mathrm{psec}),$$

where the value in [ ] is our shell-model limit one. The magnetic dipole moment of the ground state is calculated to be $\mu(1/2^+)=-0.610$ nm for which almost entire contribution comes from the Λ particle magnetic moment of the s-state (cf. Table V).

The reduced E1 transition probabilities are also estimated for the negative-parity to positive-parity cascades. Because the Λ particle has no charge, they originate from the

Table V. Magnetic moments of the hypernuclear ground states and their divided contributions from the orbital and spin parts which are given by Eqs. (3·15)~(3·18). (nm=nuclear magneton).

	J(g.s.)	μ(nm)	$\langle M_l^{\alpha x}\rangle$	$\langle M_l^{\Lambda}\rangle$	$\langle M_s^{\alpha x}\rangle$	$\langle M_s^{\Lambda}\rangle$	SUM
$^9_\Lambda$Be	$1/2^+$	−0.610	0.0	0.0	0.0	−0.730	−0.730
$^8_\Lambda$Li	1^-	0.450	0.459	0.0006	−0.184	0.263	0.538
$^7_\Lambda$Li	$1/2^+$	0.791	0.001	−0.0001	0.702	0.245	0.947
$^6_\Lambda$Li	1^-	3.322	0.909	0.0002	2.701	0.367	3.976
$^6_\Lambda$He	1^-	−1.155	0.101	0.0002	−1.850	0.367	−1.382

Table VI. Estimates of $B(E1;\,J_i^\pi\to J_f^\pi)$. ($\mathrm{e}^2\mathrm{fm}^2$).

$^9_\Lambda$Be	(L)	$J_i\to$	$(L)J_f$:	$(0^+)1/2^+$	$(2^+)3/2^+$	$(2^+)5/2^+$	$(4^+)7/2^+$
	(1^-)	$1/2^-$		0.081	0.092	—	—
		$3/2^-$		0.081	0.009	0.083	—
	(3^-)	$5/2^-$		—	0.103	0.007	0.052
	(1_2^-)	$1/2_2^-$		0.019	0.039	—	—
		$3/2_2^-$		0.019	0.004	0.035	—
$^8_\Lambda$Li		$J_i\to$	J_f:	1^-	2^-	1_2^-	0^-
		0^+		0.101	—	0.008	—
		1^+		0.004	0.064	0.032	0.011
		2^+		0.069	0.002	0.000	—
$^7_\Lambda$Li		$J_i\to$	J_f: $1/2^+$	$3/2^+$	$5/2^+$	$7/2^+$	$3/2_2^+$
		$3/2^-$	0.084	0.001	0.019	—	0.002
		$1/2^-$	0.088	0.000	—	—	0.015
		$5/2^-$	—	0.095	0.000	0.012	0.000
		$1/2_2^-$	0.000	0.098	—	—	0.001
		$3/2_2^-$	0.001	0.096	0.001	—	0.001
$^6_\Lambda$He ($^6_\Lambda$Li)		$J_i\to$	J_f: 1^-		2^-	1_2^-	
		0^+	0.069(0.155)		—	0.004(0.008)	
		1^+	0.011(0.024)		0.057(0.129)	0.003(0.006)	
		2^+	0.057(0.127)		0.004(0.004)	0.000(0.000)	

recoil of the $\alpha+\alpha$ core nucleus associated with the Λ particle transition mainly from the p-state to the s-state. Table VI lists some B(E1) estimates, which are around the Weisskopf value $B(\mathrm{E1})_W=0.055\,e^2\mathrm{fm}^2$. It is noteworthy that these values will undergo no quenching effects, because the Λ particle with zero isospin cannot excite isovector giant resonances of the core nucleus.

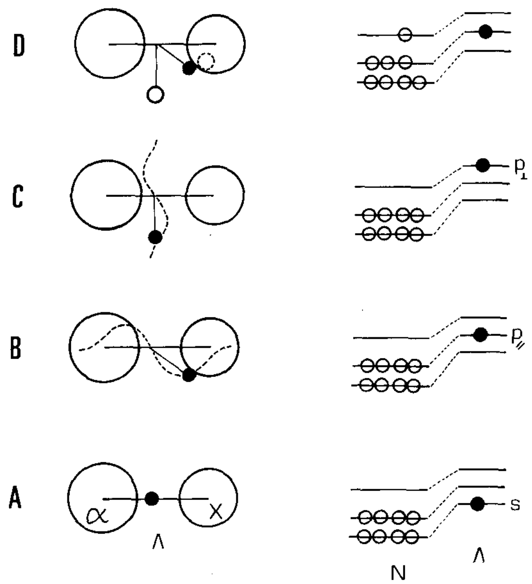

Fig. 4. Illustration of the four types of hypernuclear intrinsic structures. They are distinguished by the different configuration of the Λ particle with respect to the $\alpha+x$ core nucleus. The Λ particle (dot) occupies, respectively, (A) the s-orbit, (B) the p-orbit parallel to the α-x deformation axis, (C) the p-orbit perpendicular to the α-x axis, and (D) the $p(s)$-orbit. In the last case (D), a nucleon-hole is in the $x(\alpha)$ cluster and a nucleon outside the two nuclear clusters. The corresponding shell-model pictures (for the $^9_\Lambda$Be case) are shown on the right side.

Let us discuss the three-band level structure in relation to the peaks observed in the $^9\mathrm{Be}(K^-, \pi^-)\,^9_\Lambda\mathrm{Be}$ reaction.[1)~4)] In Fig. 4 we depict the cluster model illustrations of four types of intrinsic structures of hypernuclear states, where x means the α cluster in the present case. To help understanding we also draw the corresponding shell-model configurations, where the p-state splits into the $p_{/\!/}$- and $p_\perp$-orbitals which are parallel and perpendicular to the deformation axis, respectively. The ground $K=0^+$ band has evidently the A-type structure in which the Λ particle occupies the s-state with respect to the ^{8}Be core. So we call this band the "^{8}Be-analog band". It is noted that our $K=1^-$ band having the C-type structure is similar to the ground band of ^{9}Be, except the sizable spin-orbit splittings in the latter. Thus this band may be called the "^{9}Be-analog band". The $3/2^-$ member of this band can be reached by a simple substitution of the last odd neutron in $^9\mathrm{Be}(3/2_g^-)$ by the Λ particle. The big peak observed at $B_\Lambda^{\exp}=-6.3$ MeV is, therefore, identified as our $3/2_2^-(L=1_2^-)$ level ($B_\Lambda=-5.31$ MeV). In fact the calculated effective neutron numbers $N_{\mathrm{eff}}(i\to f;$

Table VII. Calculated effective neutron numbers $N_{\mathrm{eff}}(\theta=0°)$ for the (K^-, π^-) reactions with $p_K=720$ MeV/c. Pure imaginary optical potentials for K^- and π^- are used with $\bar\sigma_{KN}=\bar\sigma_{\pi N}=30$ mb.

$^9_\Lambda$Be		$^7_\Lambda$Li		$^6_\Lambda$Li	
L	$N_{\mathrm{eff}}(0°)$	J	$N_{\mathrm{eff}}(0°)$	J	$N_{\mathrm{eff}}(0°)$
0^+	0.002	$1/2^+$	0.011	1^-	0.002
2^+	0.002	$3/2^+$	0.000	2^-	0.010
1^-	0.010	$5/2^+$	0.012	1_2^-	0.004
3^-	0.002	$3/2^-$	0.892	0^-	0.001
1_2^-	0.354	$1/2^-$	0.004	1^+	0.413
2^-	0.070	$3/2_2^-$	0.006	2^+	0.001
				3^+	0.006
$N_{\mathrm{eff}}^{\mathrm{tot}}(0°)$	2.18		1.75		1.41

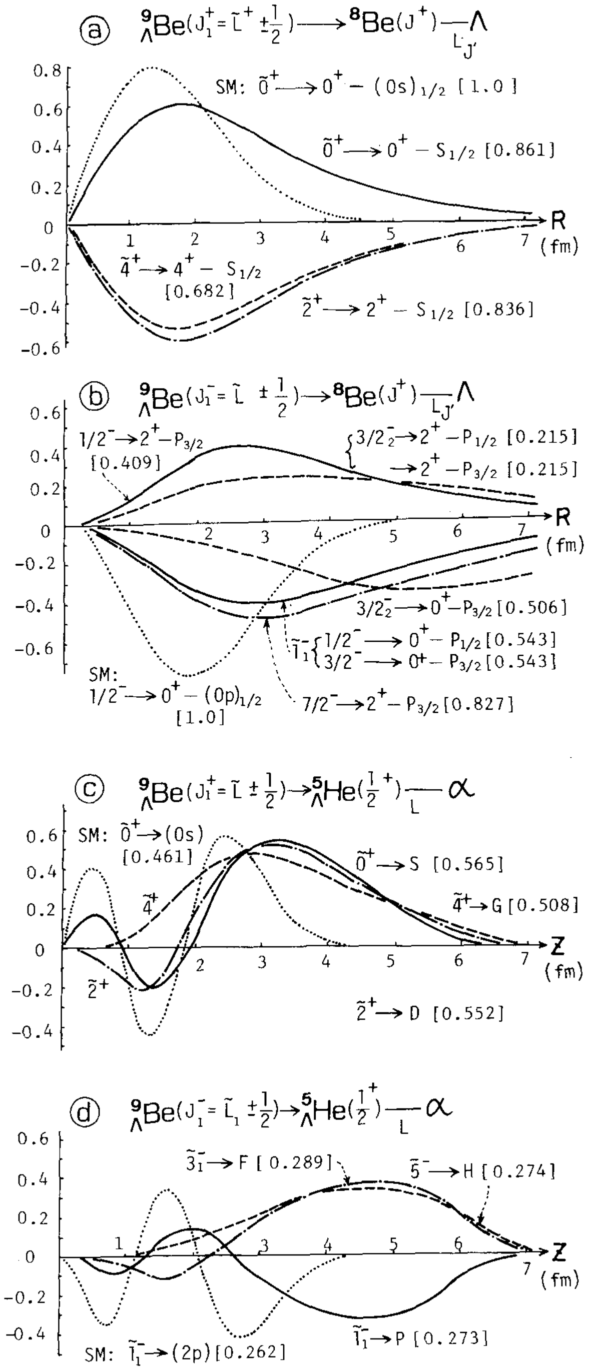

Fig. 5. The reduced width amplitudes (RWA) of ${}^{9}_{\Lambda}$Be as a function of the relative distance (R or Z) between the two fragments. The corresponding spectroscopic factors are given in [ ] after the indicated decay channels. For comparison the typical shell-model (SM) RWA are drawn by dotted lines.

$\theta=0$) exclusively concentrate on the $3/2_2^-(L=1_2^-)$ level as seen in Table VII.

The $K=0^-$ band has the B-type intrinsic structure of Fig. 4 and can never appear in the ordinary nucleus because of the Pauli exclusion principle. For this reason we call these states "genuinely hypernuclear". The Λ particle in the B-type structure occupies the same orbital space as that of the maximum symmetric nucleons in the α cluster. In the shell-model limit, therefore, our $K=0^-$ wf tends to the configuration with an $SU(3)$ classification $[f](\lambda\mu)=[54](50)$ which was called "supersymmetric" by Dalitz and Gal.[21] The band head $L=1_1^-$ level has not been seen yet as a peak probably being hidden by the tail of the big $L=1_2^-$ peak. By improving the experimental condition and/or measuring the pion angular distribution, this "genuinely hypernuclear" state should be able to come into observation.

Another strong peak observed at $B_\Lambda^{\text{exp}}=-17$ MeV[4] can be assigned to have the configuration of D-type which is generated by the recoilless conversion of a neutron in the deeper p (and s)-orbit to Λ. The D-type configuration may be obtained from the B-type by exciting a neutron from the deeper p-orbit to the upper one (cf. Fig. 4). The energy spacing between the two p-orbits for nucleon is known experimentally to be about 17 MeV, hence the observation of the strong peak at $B_\Lambda^{\text{exp}}=-17$ MeV is consistent with our prediction of the B-type $(K=0)$ 1_1^- level at $B_\Lambda=-0.03$ MeV. The D-type configuration itself is, however, not within our present $\alpha+\alpha+\Lambda$ model space. In Table VIII are summarized the calculated and observed B_Λ values of the hypernuclear ground states and some excited states strongly populated in the (K^-, π^-) reactions.

Figure 5 displays the reduced width

Table VIII. Λ-particle binding energies (B_Λ) in the hypernuclear ground state[35] and some excited states strongly populated in the (K^-, π^-) reactions.[1)~5)] (MeV)

	peak :	small(g.s.)		large		large
${}^9_\Lambda$Be	Exp	6.71±0.04	*		−6.3±	−17.0±
	Cal	7.49(1/2⁺)	−0.03(1/2, 3/2₁⁻)		−5.31(3/2₂⁻)	Δ
${}^8_\Lambda$Li	Exp	6.80±0.03	*		*	*
	Cal	7.20(1⁻)	−0.21(0⁺)		−3.03(2⁺)	Δ
${}^7_\Lambda$Li	Exp	5.58±0.03		−2.7±		−14.6±
	Cal	5.59(1/2⁺)		−3.10(3/2⁻)		Δ
${}^6_\Lambda$Li	Exp	4.5±0.5**		−3.8±		−13.8±
	Cal	3.97(1⁻)		−4.07(1⁺)		Δ

* Not observed. ** 4.25±0.1 MeV for ${}^5_\Lambda$He. Δ Out of the present model space.

Table IX. Estimates of partial decay widths Γ_c of the typical resonance states. The separation energy method is employed. For definitions see Eq. (3·30) and (3·31).

	J	B_Λ(MeV) [B_Λ^{exp}]	decay channels	S^2factor	radius a(fm)	P	γ_W^2 (MeV)	θ^2	Γ_c (MeV)
${}^9_\Lambda$Be	$1/2^-$	(−0.03)	^{8}Be(0⁺)-Λ($P_{1/2}$)	0.543	3.5	0.23	4.29	0.19	0.42
		[*]	${}^5_\Lambda$He(1/2⁺)-α(${}^1P_1$)	0.273	5.0	2.81	1.10	0.15	0.93
	$3/2_2^-$		^{8}Be(0⁺)-Λ(P3/2)	0.506	6.0	3.03	1.67	0.25	2.53
		(−5.31)	^{8}Be(2⁺)-Λ($P_{3/2}$)	0.215	4.5	1.37	2.91	0.10	0.80
		[−6.3]	^{8}Be(2⁺)-Λ($P_{1/2}$)	0.215	4.5	1.37	2.91	0.10	0.80
			${}^5_\Lambda$He(1/2⁺)-α(${}^1P_1$)	0.266	5.0	3.15	1.10	0.15	1.04
${}^7_\Lambda$Li	$3/2^-$	(−3.10)	^{6}Li(1⁺)-Λ($P_{3/2}$)	0.412	5.5	1.84	2.08	0.17	1.26
		[−2.7]	^{6}Li(1⁺)-Λ($P_{1/2}$)	0.441	5.5	1.84	2.08	0.17	1.26
			^{6}Li(3⁺)-Λ($P_{3/2}$)	0.120	4.0	0.52	3.83	0.03	0.12
			${}^5_\Lambda$He(1/2⁺)-d(${}^3P_2$)	0.132	5.0	2.53	1.73	0.07	0.58
${}^6_\Lambda$Li	1^+	(−4.07)	^{5}Li(3/2⁻)-Λ($P_{3/2}$)	0.557	5.5	1.94	2.15	0.23	1.90
		[−3.8]	^{5}Li(3/2⁻)-Λ($P_{1/2}$)	0.433	5.5	1.94	2.15	0.12	0.99
			^{5}Li(1/2⁻)-Λ($P_{3/2}$)	0.008	5.0			0.00	0.00
			${}^5_\Lambda$He(1/2⁺)-p($S_{1/2}$)	0.058	6.0	3.37	2.06	0.03	0.33

* Not observed.

amplitudes (RWA) and spectroscopic factors leading to the ${}^5_\Lambda$He-α and ^{8}He-Λ channels. Though the cluster-model S-factor does not differ so much from the corresponding shell-model limit one, the cluster-model relative wf extends to much larger distance. In Table IX we show some partial decay widths evaluated on the basis of the separation energy method desribed in § 3.3. From these we have a rough estimate of the total widths, $\Gamma(1/2_1^-)=1.0\sim1.4$ MeV and $\Gamma(3/2_2^-)=3.0\sim5.2$ MeV, the latter of which seems a bit smaller than the strong peak width observed at $B_\Lambda^{exp}=-6.3$ MeV in the (K^-, π^-) reac tion.[1)~5)] Table X lists the ho expansion of the typical Λ particle wf's in each dominant angular momentum channel. One can see that the s-state Λ-particle wf generally concentrates on the lowest two ho states, while the p-state wf is scattered over several ho states with the components depending on the level energy.

4.2. *The hypernucleus* ${}^8_\Lambda$*Li*

The calculated energy spectra of ${}^8_\Lambda$Li are shown in Figs. 6 and 7. In Fig. 6 dominant

Table X. Harmonic oscillator expansions of the Λ-particle wave functions $\chi_\lambda^\Lambda(R)$ in the dominant channel of some typical states. The channel is expressed by $(l\lambda)_L^S$ with its occupancy(%) in the total hypernuclear wf. Entries are $a_{K\lambda}^2$ of $\chi_\lambda^\Lambda(R)=\sum_K a_{K\lambda} u_{K\lambda}(R)$ where $K=2\nu+\lambda$ and $0\leq\nu\leq 9$. Negligibly small numbers are represented by dots.

	${}^9_\Lambda$Be			${}^8_\Lambda$Li		${}^7_\Lambda$Li		${}^6_\Lambda$He(${}^6_\Lambda$Li)	
J	$1/2^+$	$3/2^-$	$3/2_2^-$	1^-	0^+	$1/2^+$	$3/2^-$	1^-	0^+
E	−7.12	0.40	5.68	−10.76	−3.34	−7.09	1.88	−2.84	4.95
$(l\lambda)_L^S$	$(00)_0^{1/2}$	$(01)_1^{1/2}$	$(01)_1^{1/2}$	$(10)_1^0$	$(11)_0^0$	$(00)_0^{1/2}$	$(01)_1^{1/2}$	$(10)_1^0$	$(11)_0^0$
(%)	94.5	54.9	53.6	88.5	98.0	98.5	84.9	68.8	75.9
χ_λ^Λ	s	p	p	s	p	s	p	s	p
$\nu=0$	.838	.547	.085	.877	.600	.870	.331	.854	.277
$\nu=1$	.113	.226	.145	.081	.194	.076	.198	.073	.189
$\nu=2$	.031	.102	.185	.027	.091	.034	.156	.044	.167
$\nu=3$	:	.057	.179	:	.052	:	.116	:	.130
$\nu=4$	:	.033	.153	:	.029	:	.088	:	.097
$\nu=5$	:	:	.114	:	:	:	.055	:	.066

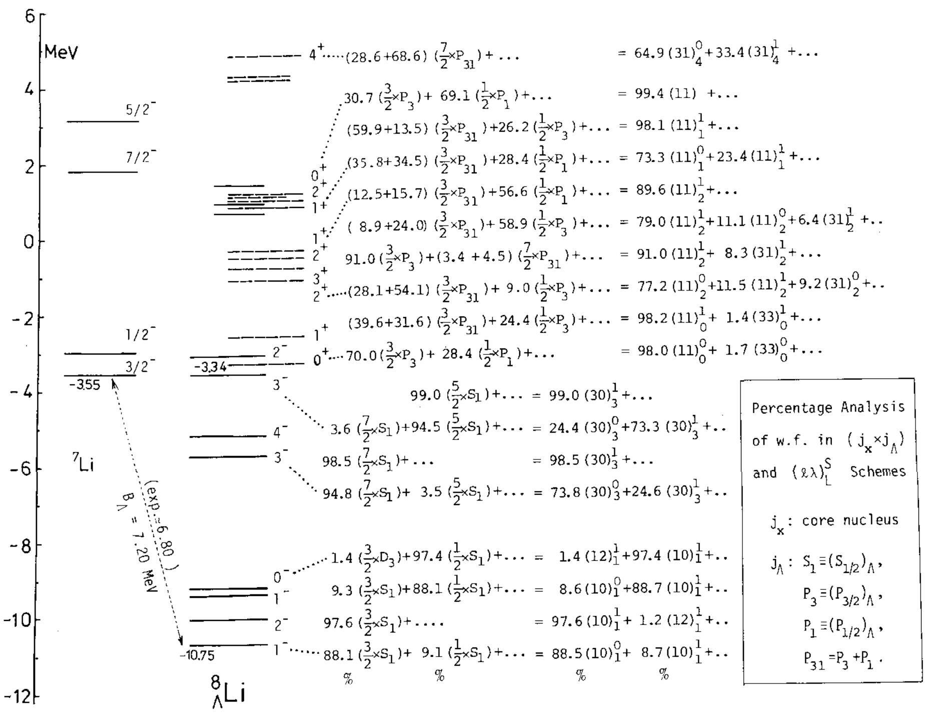

Fig. 6. Calculated energy spectra of ^{7}Li and ${}^8_\Lambda$Li. Comments as for Fig. 2 except that the wave functions are given in both the j_x-j_Λ and L-S coupling schemes.

components of their wf's are expressed in the j_x-j_Λ and L-S coupling schemes. Based on the lowest four levels of ^{7}Li, the 8 negative parity states are grouped into four doublets: 1^--2^-, 1^--0^-, 3^--4^- and 3^--2^-. Each wf has the structure $[(lj_x)\times s_{1/2}^\Lambda]$ where the Λ particle in the $\lambda j_\Lambda=s_{1/2}^\Lambda$ state weakly couples to one of the α-t di-cluster states with $lj_x=P_{3/2}$, $P_{1/2}$, $F_{7/2}$ and $F_{5/2}$, respectively. These low-lying negative parity states correspond to the A-type intrinsic cluster structure of Fig. 4 $(x=t)$. It is interesting to note that the Λ-N

interaction gives rise to such mixings in the j_x-j_Λ coupling scheme as to recover the spatial symmetry (L-S coupling) of the hypernuclear system. This feature is seen from, for example, the fact that the 1_1^- wf has the 88.5% $(l\lambda)_L{}^S=(10)_1{}^0$ component in the L-S coupling scheme, which is much larger than the occupancy (66.7%) contained in the pure j_x-j_Λ coupling configuration $[3/2^-\times s_{1/2}^\Lambda]$. The calculated ground state binding energy $B_\Lambda=7.20$ MeV is somewhat larger than the observed value $B_\Lambda{}^{\exp}=6.80$ MeV.[35)]

We obtain many positive parity levels in which the Λ particle mainly occupies the p-state ($\lambda=1$) with respect to the core nucleus ^{7}Li. The B-type and C-type intrinsic structures of Fig. 4 ($x=t$) are underlying for these levels, hence the spectra are naturally expected to be analogous to those of ^{8}Be($K=0^+$) and ^{8}Li($K=1^+$). In the hypernuclear $\alpha+t+\Lambda$ system, however, we have two possible spin values ($S=0$ and 1) with essentially the same spatial structure. Thus, in terms of the strong coupling L-S scheme, a transparent interpretation may be given to the four "bands", i.e. $K=0^+$ and 1^+ with $S=0$ and 1:

(i) Spin-singlet($S=0$) ^{8}Be-analogs: $J=0^+, 2^+, 4^+$,
(ii) Spin-triplet($S=1$) ^{8}Be-analogs: $J=1^+$; $\{1^+, 2^+, 3^+\}$, $\{3^+, 4^+, 5^+\}$,
(iii) Spin-singlet($S=0$) ^{8}Li-analogs: $J=1^+, 2^+, 3^+, \cdots$,
(iv) Spin-triplet($S=1$) ^{8}Li-analogs: $J=\{0^+, 1^+, 2^+\}$, $\{1^+, 2^+, 3^+\}, \cdots$.

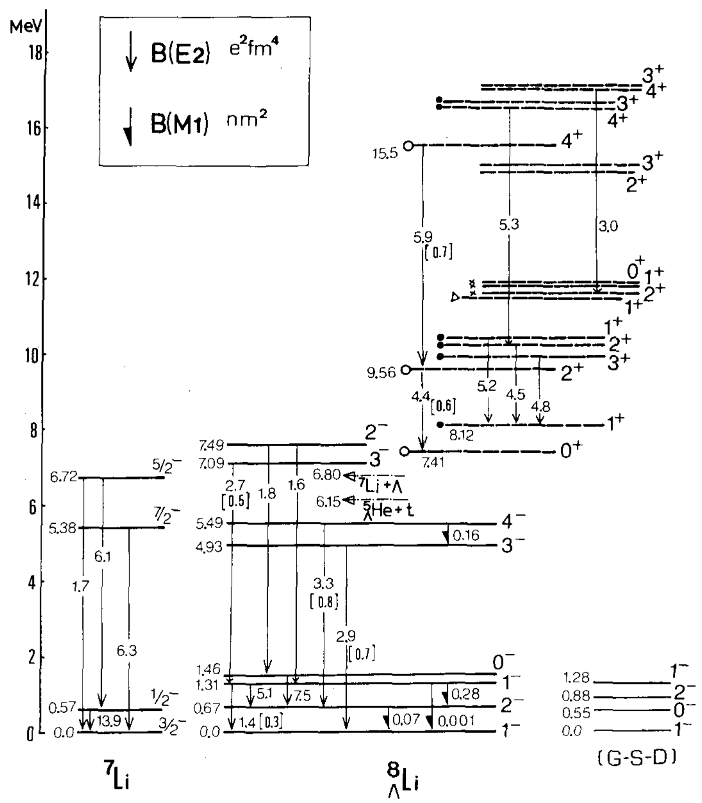

Fig. 7. Calculated B(E2) and B(M1) in ^{7}Li and $^8_\Lambda$Li. The levels with a similar character are indicated by open circle, dot, etc. The experimental threshold energies are indicated in the $^8_\Lambda$Li spectrum. The shell-model limit B(E2) values are in the square brackets. The levels predicted by Gal et al. (G-S-D)[11)] are compared. See the text for more detail.

In fact the first 0^+-2^+-4^+ band is realized as marked by open circle (○) in Fig. 7. The predominant component of their wf's is $(l\lambda)_L{}^S=(l1)^0_{0,2,4}$, respectively, and therefore this band is regarded to have the di-cluster intrinsic structure (B-type) with $\alpha+{}^4_\Lambda\mathrm{He}(0^+)$ as is analogous to $^8\mathrm{Be}=\alpha+\alpha$. The low-lying levels of the spin-triplet ^{8}Be-analogs which could be said "genuinely hypernuclear" are indicated by dot (●) in Fig. 7. The intrinsic structure of this band is also the B-type whose wf has the $S=1$ dominant component $(l\lambda)_L{}^S=(l1)^1_{0,2,4}$. It is noted, however, that the Λ particle does not always move around the t cluster, but moves in parallel with the α-t deformation axis. Further understanding of this feature can be achieved by comparing two kinds of spectroscopic factors leading to the α-${}^4_\Lambda$H ad ${}^5_\Lambda$He-t decay channels. From Table XI we see that, in the ^{8}Be-analog bands $(S=0,1)$, the S-factor to the α-${}^4_\Lambda$H channel is larger than the other in spite of the fact: $B_\Lambda{}^{\mathrm{cal}}({}^4_\Lambda\mathrm{H})=1.08$ MeV vs $B_\Lambda{}^{\mathrm{cal}}({}^5_\Lambda\mathrm{He})=3.12$ MeV. Thus the simple picture mentioned above

Table XI. Spectroscopic factors of the ^{8}Li states leading to the indicated three channels.

$J({}^8_\Lambda\mathrm{Li})$	${}^5_\Lambda\mathrm{He}(1/2)-t$ (L_J)	$\alpha-{}^4_\Lambda\mathrm{He}(J_x)$ $(l\text{-}J_x)$	$^7\mathrm{Li}-\Lambda$ $(j_x\text{-}\lambda j_\Lambda)$
1^-	0.786 ($P_{3/2}$)	0.616 (P-0^+)	0.831 ($3/2$-$s_{1/2}$)
	0.082 ($P_{1/2}$)	0.056 (P-1^+)	0.085 ($1/2$-$s_{1/2}$)
2^-	0.872 ($P_{3/2}$)	0.633 (P-1^+)	0.926 ($3/2$-$s_{1/2}$)
$1_2{}^-$	0.792 ($P_{1/2}$)	0.585 (P-1^+)	0.831 ($1/2$-$s_{1/2}$)
	0.083 ($P_{3/2}$)		0.088 ($3/2$-$s_{1/2}$)
0^-	0.875 ($P_{1/2}$)	0.644 (P-1^+)	0.922 ($1/2$-$s_{1/2}$)
0^+	0.281 ($S_{1/2}$)	0.338 (S-0^+)	0.695 ($3/2$-$p_{3/2}$)
			0.282 ($1/2$-$p_{1/2}$)
1^+	0.274 ($S_{1/2}$)	0.312 (S-1^+)	0.314 ($3/2$-$p_{1/2}$)
			0.243 ($1/2$-$p_{3/2}$)
			0.394 ($3/2$-$p_{3/2}$)
2^+	0.234 ($D_{5/2}$)	0.297 (D-0^+)	0.539 ($3/2$-$p_{1/2}$)
		0.041 (D-1^+)	0.280 ($3/2$-$p_{3/2}$)
3^+	0.248 ($D_{5/2}$)	0.316 (D-1^+)	0.909 ($3/2$-$p_{3/2}$)
4^+	0.266 ($G_{9/2}$)	0.300 (G-0^+)	0.685 ($7/2$-$p_{1/2}$)
			0.909 ($7/2$-$p_{3/2}$)
Shell-model limit: (J^-)	0.874		1.0
(J^+)	0.343		

Table XII. Root mean square estimates of the α-t and ^{7}Li-Λ distances in ${}^8_\Lambda$Li as compared with that of ^{7}Li. Note that $\sqrt{\langle r^2\rangle_\alpha}=1.440$ fm and $\sqrt{\langle r^2\rangle_t}=1.358$ fm with $b=1.358$ fm.

(fm)

^{7}Li			${}^8_\Lambda$Li							
J	$\sqrt{\langle r^2\rangle_{\alpha\text{-}t}}$	Tot	J	$\sqrt{\langle r^2\rangle_{\alpha\text{-}t}}$	$\sqrt{\langle R^2\rangle}$	Tot	J	$\sqrt{\langle r^2\rangle_{\alpha\text{-}t}}$	$\sqrt{\langle R^2\rangle}$	Tot
$3/2^-$	3.51	2.24	1^-	3.08	2.31	2.08	0^+	3.62	3.65	2.45
			2^-	3.10	2.35	2.10	1^+	3.63	3.82	2.48
							2^+	3.53	4.16	2.51
$1/2^-$	3.60	2.27	$1_2{}^-$	3.17	2.38	2.12	$1_3{}^+$	3.48	5.04	2.67
			0^-	3.17	2.39	2.12	$2_3{}^+$	3.48	5.10	2.68
$7/2^-$	3.32	2.16	3^-	2.81	2.21	1.99				
$5/2^-$	3.59	2.27	$3_2{}^-$	2.96	2.30	2.05				

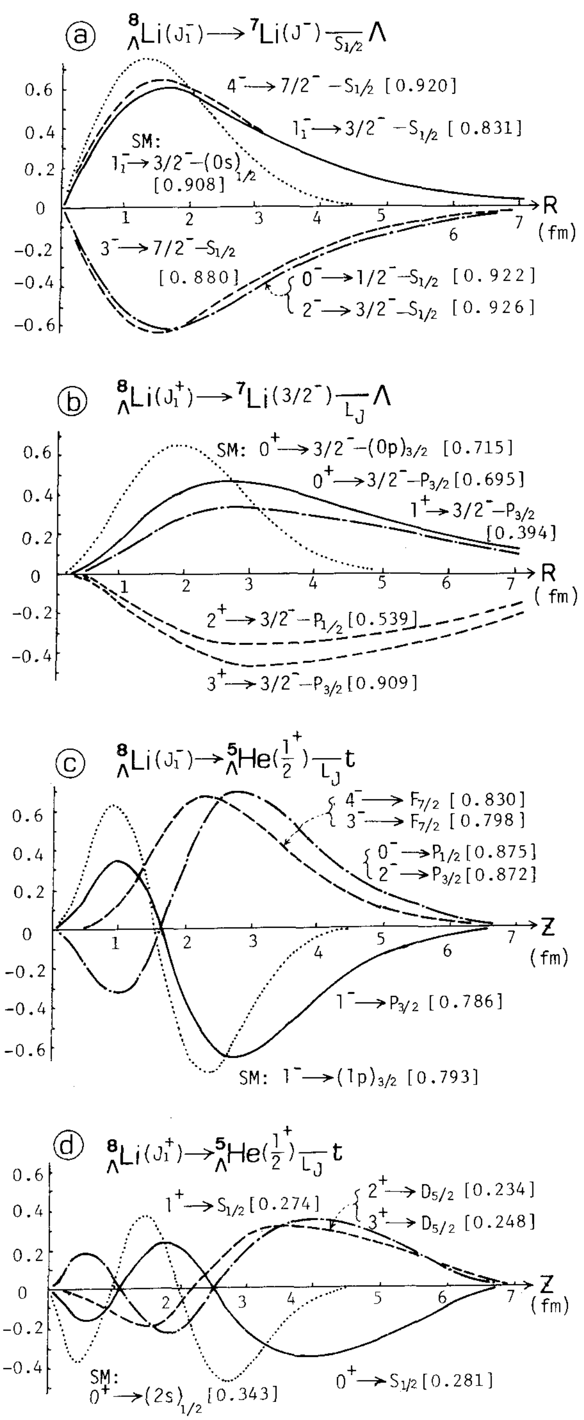

Fig. 8. RWA of ${}^{8}_{\Lambda}$Li. Comments as for Fig. 5.

persists to characterize the band structures.

The element characterizing the other two bands is the C-type intrinsic structure ($K=1^+$) in which the last odd neutron in ^{8}Li$=\alpha+t+n$ is substituted by the Λ particle. In Fig. 7 we show only a few corresponding analog states with $S=0$ by triangle (△) and those with $S=1$ by cross (×).

Estimates of the reduced E2 transition probabilities B(E2) are summarized in Fig. 7 where some B(M1) predictions are also given. Bedjidian et al.[8] reported the observation of 1.22 MeV γ-ray from ${}^{8}_{\Lambda}$Li suggesting the M1 transition of $1_2^-\to 1_1^-$. Here we get the comparable energy difference 1.31 MeV and the transition rates:

$$T(\mathrm{M1};\,1_2^-\to 1^-)=3.96\times 10^{10}\ \mathrm{sec}^{-1};$$
$$B(\mathrm{M1})=0.001\ \mathrm{nm}^2,$$
$$T(\mathrm{E2};\,1_2^-\to 1^-)=6.59\times 10^{9}\ \mathrm{sec}^{-1};$$
$$B(\mathrm{E2})=1.4\ e^2\mathrm{fm}^4[\,0.3\ e^2\mathrm{fm}^4],$$

where [ ] is our shell-model limit value. Thus, being consistent with their suggestion, the M1 transition is predicted to occur more than 6 times faster than the E2 transition. Another possible transition $1_2^-\to 2^-$ may not likely be the candidate for the observed γ-ray because the energy difference is obtained to be too small (0.64 MeV). However the deduced M1 transition rate is much stronger than the former:

$$T(\mathrm{M1};\,1_2^-\to 2^-)=1.29\times 10^{12}\ \mathrm{sec}^{-1};$$
$$B(\mathrm{M1})=0.28\ \mathrm{nm}^2,$$
$$T(\mathrm{E2};\,1_2^-\to 2^-)=6.68\times 10^{8}\ \mathrm{sec}^{-1};$$
$$B(\mathrm{E2})=5.1\ e^2\mathrm{fm}^4[\,1.2\ e^2\mathrm{fm}^4].$$

Compared with our shell model limit B(E2) values, the cluster model estimates are about 4(8) times enhanced within the negative (positive) parity states. We can also recognize from Table XII that the α-t r.m.s. distance in each of the negative parity states in ${}^{8}_{\Lambda}$Li is more than 10% contracted from that in ^{7}Li. This is responsible for the reduction of the B(E2) strengths in comparison with those in ^{7}Li.

The magnetic dipole moment of the ground state is calculated to be $\mu(1^-,{}^{8}_{\Lambda}\mathrm{Li})=0.450$

nm, to which the core nucleus and the Λ particle equally contribute (cf. Table V). Table VI lists B(E1) values predicted for some $J^+ \to J^-$ transitions. They do not differ so much from the Weisskopf estimate $B(\mathrm{E1}, {}^{8}_{\Lambda}\mathrm{Li})_W = 0.036\ e^2\mathrm{fm}^2$.

The RWA leading to the ^{7}Li-Λ and $^5_\Lambda$He-t channels are drawn in Fig. 8 as a function of the distance between the two fragments. The typical shell-model limit RWA are displayed for comparison. One can see that behaviors of the two kinds of RWA differ appreciably.

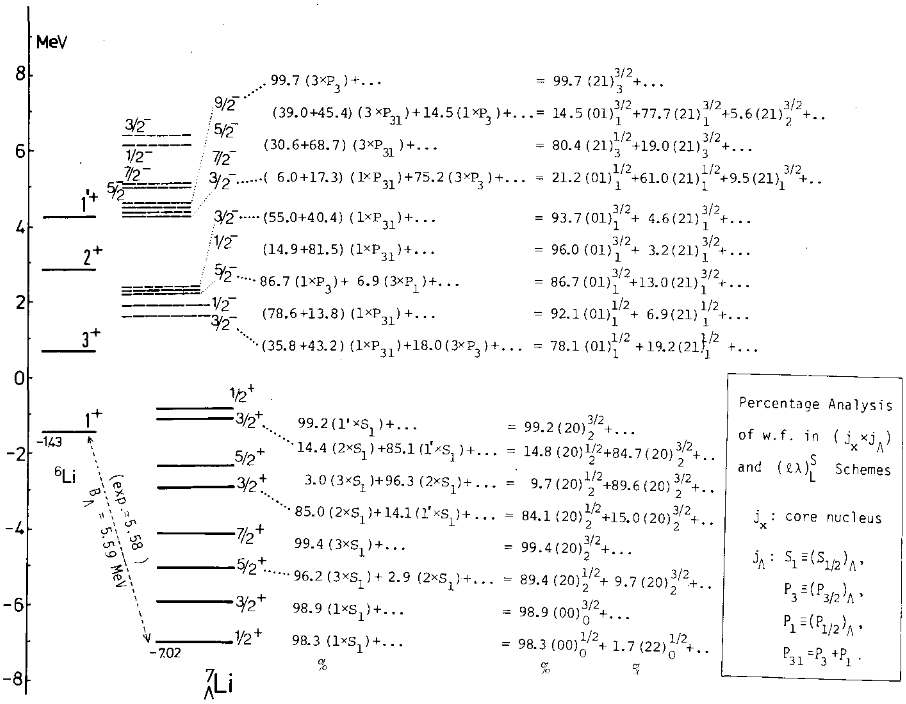

Fig. 9. Calculated energy spectra of ^{6}Li and $^7_\Lambda$Li. Comments as for Fig. 6.

4.3. *The hypernucleus $^7_\Lambda$Li*

The calculated energy spectra of $^7_\Lambda$Li are shown in Fig. 9 with the dominant wf components and also in Fig. 10. The coupling $[{}^6\mathrm{Li}(lj_x) \times s^{\Lambda}_{1/2}]$ with $lj_x = S1^+$, $D3^+$, $D2^+$ and $D1^+$ provides low-lying four positive parity doublets. The intrinsic cluster structure of these states clearly manifests the A-type in Fig. 4 ($x=d$). As the $^5_\Lambda$He-d threshold energy is experimentally 3.94 MeV above the ground state, we have four particle-stable bound states with $B_\Lambda(g.s.) = 5.59$ MeV being in good agreement with $B_\Lambda^{\exp} = 5.58$ MeV.[35] Reflecting the weak coupling feature in these 8 positive parity states, they are well described by a single configuration in the j_x-j_Λ couling scheme (cf. Fig. 9). Note that the energy level splittings in ^{6}Li are very large and the Λ-N interaction is not strong enough to give rise to the sizable $\Delta l = 2$ coupling. In each doublet, the $\boldsymbol{\sigma}_\Lambda \cdot \boldsymbol{\sigma}_N$ interaction lowers in energy the member with the dominant $S_< = 1/2$ component.

Very recently 2 MeV γ-ray was observed at BNL[9] and interpreted to come from the $5/2^+ \to 1/2^+$ transition. Our result for the transition energy is 1.99 MeV, which is just in good agreement with the experiment. Note that the observed levels of the ^{6}Li core nucleus are very well reproduced by the present α-d model. The $5/2^+$-$1/2^+$ and $7/2^+$-$3/2^+$

energy splittings appear to be parallel to the corresponding nuclear 3^+-1^+ splitting(Cal. 2.13 MeV). It is interesting, however, to remark that these splittings are obtained to be slightly compressed due to the different responses of the 3^+ and 1^+ α-d wf's against the addition of the Λ particle.

Bunched energy levels are obtained for the negative parity states in which the Λ particle is dominantly in the p-state. The states in the lowest bunch are constructed from the coupling $[{}^6\mathrm{Li}(1^+)\times\{p^{\Lambda}_{1/2}, p^{\Lambda}_{3/2}\}]$, and those in the next bunch $[{}^6\mathrm{Li}(3^+)\times\{p^{\Lambda}_{1/2}, p^{\Lambda}_{3/2}\}]$, etc. The classification according to the intrinsic cluster structures given in Fig. 4 $(x=d)$ is also approximately valid for these levels. Considering two possible spin values, the wf analysis allows one to rearrange them into the following four groups:

(i) Spin-doublet $(S=1/2)$ ^{7}Li-analogs: $J=\{1/2^-, 3/2^-\}$, $\{5/2^-, 7/2^-\}$,
(ii) Spin-quartet $(S=3/2)$ ^{7}Li-analogs: $J=\{1/2^-, 3/2^-, 5/2^-\}$, $\{3/2^-, 5/2^-, 7/2^-, 9/2^-\}$,
(iii) Spin-doublet $(S=1/2)$ ^{7}Li*-analogs,
(iv) Spin-quartet $(S=3/2)$ ^{7}Li*-analogs.

Here we use the notation '^{7}Li-' for the lowest four states in ^{7}Li describable with the $\alpha+t$ di-cluster and the notation '^{7}Li*-' for the other excited states having three-body structure such as $\alpha+d+n$. The spectrum of the first group, as marked by open circle (○) in Fig. 10, is in fact analogous to the $^7\mathrm{Li}=\alpha+t$ spectrum but with some compression. Thus the spin-doublet ^{7}Li-analogs are simply regarded to have the B-type intrinsic structure in Fig. 4.

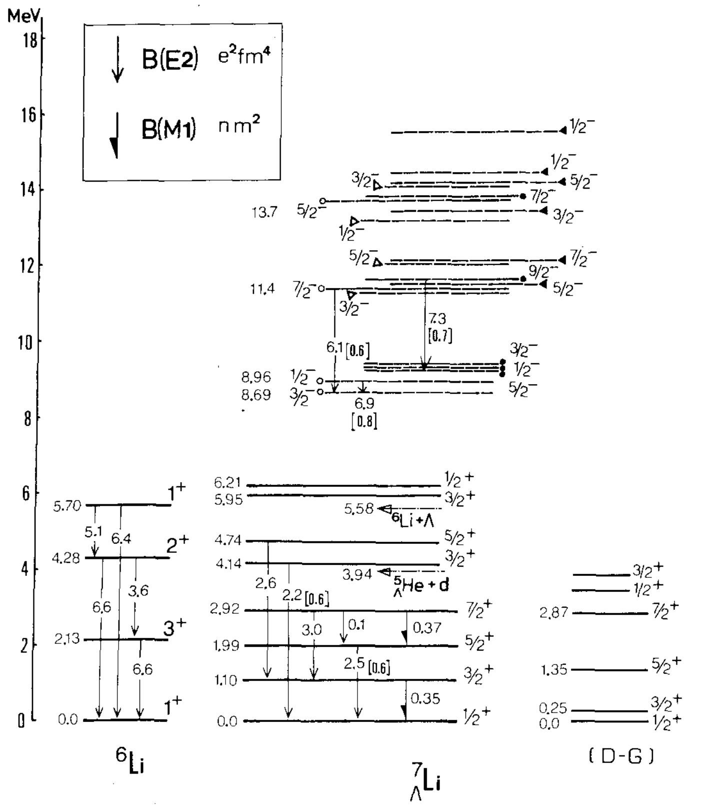

Fig. 10. Calculated B(E2) and B(M1) in ^{6}Li and $^7_\Lambda$Li. The spectrum obtained by Dalitz and Gal (D-G)[15] is shown for comparison. Comments as for Fig. 7.

The second spectrum may have the B-type one with the coupling $[(L=1\,\&\,3)\times(S=3/2)]$. They are indicated by dot (●) in Fig. 10. It should be remarked that nearly degenerate appearance of these two groups having different spin values is one of the characteristics of the hypernuclear spectra. The states belonging to the third and fourth groups appear at higher excitation energies.

The Heidelberg-Saclay-Strasbourg Collaboration[1)~5)] found two large peaks at $B_\Lambda^{\rm exp}=-2.7$ MeV and -14.6 MeV in the forward ^{7}Li$(K^-,\pi^-)^7_\Lambda$Li reaction. The other small peak at $B_\Lambda^{\rm exp}=5.6$ MeV reasonably corresponds to the $^7_\Lambda$Li ground state. The two strong peaks have been ascribed to the substitutional configurations $(\Lambda p_{3/2},\nu p_{3/2}^{-1})$ and $(\Lambda s_{1/2},\nu s_{1/2}^{-1})$, respectively, produced by the recoilless Λ-production. In the present investigation the large peak at $B_\Lambda^{\rm exp}=-2.7$ MeV is identified with our $3/2^-$ level obtained at $B_\Lambda=-3.10$ MeV which is an analog of the target ground state ^{7}Li$(3/2_g^-)$. Calculated $N_{\rm eff}$ for the reaction in Table VII supports this interpretation. Description of the other large peak may involve a neutron hole in the α cluster, which is out of the present model space.

The calculated B(E2) values are displayed in Fig. 10, which support as a whole the classification of the spectra discussed above. From typical B(E2) estimates we see that the enhancements with respect to our shell-model limit are about 3 (8) times in the positive (negative) parity states. Dalitz and Gal deduced the E2 transition rates for $5/2^+\to3/2^+$ and $5/2^+\to1/2^+$ on the assumption that both uniquely involve the core transition ^{6}Li$(3^+\to1^+)$ with the observed rate $T({\rm E2})=6.7\times10^{11}$ sec^{-1}. Their values are very large in comparison with ours:

$$T({\rm E2};\,5/2^+\to3/2^+)=2.7\times10^8\ {\rm sec}^{-1};\qquad B({\rm E2})=0.4\ e^2{\rm fm}^4(\text{ D-G}: 3.1\ e^2{\rm fm}^4),$$
$$T({\rm E2};\,5/2^+\to1/2^+)=9.5\times10^{10}\ {\rm sec}^{-1};\qquad B({\rm E2})=2.5\ e^2{\rm fm}^4(\text{ D-G}: 8.6\ e^2{\rm fm}^4).$$

This difference arises because the dynamical contraction of the α-d distance due to the addition of the Λ particle is naturally taken into account here. This effect, as shown in Table XIII, is so remarkable as to reduce the hypernuclear B(E2) values to nearly half the core nuclear ones. On the other hand our B(E2) predictions are underestimated, since the present ^{6}Li wf's yield $B({\rm E2};\,3^+\to1^+)=6.6\ e^2{\rm fm}^4$ without additional effective charge while $11.0\ e^2{\rm fm}^4$ is obtained experimentally. Thus the reasonable B(E2) values in $^7_\Lambda$Li should be nearly 1.5 times the values shown in Fig. 10.

Table XIII. Root mean square estimates of the α-d and ^{6}Li-Λ distances in $^7_\Lambda$Li as compared with that of ^{6}Li. Note that $\sqrt{\langle r^2\rangle_\alpha}=1.440$ fm and $\sqrt{\langle r^2\rangle_d}=1.176$ fm with $b=1.358$, fm. (fm)

^{6}Li			$^7_\Lambda$Li							
J	$\sqrt{\langle r^2\rangle_{\alpha\text{-}d}}$	Tot	J	$\sqrt{\langle r^2\rangle_{\alpha\text{-}d}}$	$\sqrt{\langle R^2\rangle_\Lambda}$	Tot	J	$\sqrt{\langle r^2\rangle_{\alpha\text{-}d}}$	$\sqrt{\langle R^2\rangle_\Lambda}$	Tot
1^+	3.80	2.14	$1/2^+$	3.13	2.40	2.04	$3/2^-$	3.80	4.49	2.61
			$3/2^+$	3.21	2.50	2.08	$1/2^-$	3.79	4.67	2.64
							$5/2^-$	3.80	4.79	2.67
							$1/2^-$	3.80	4.89	2.70
							$3/2_2^-$	3.78	4.91	2.69
3^+	3.66	2.08	$5/2^+$	2.91	2.33	1.96	$3/2_3^-$	3.64	5.06	2.69
			$7/2^+$	2.98	2.42	2.00	$7/2^-$	3.66	4.87	2.65
							$5/2_2^-$	3.66	5.06	2.70
							$9/2^-$	3.67	4.97	2.68
2^+	3.63	2.07	$3/2_2^+$	2.85	2.31	1.94				
1_2^+	3.61	2.06	$3/2_3^+$	2.87	2.37	1.96				

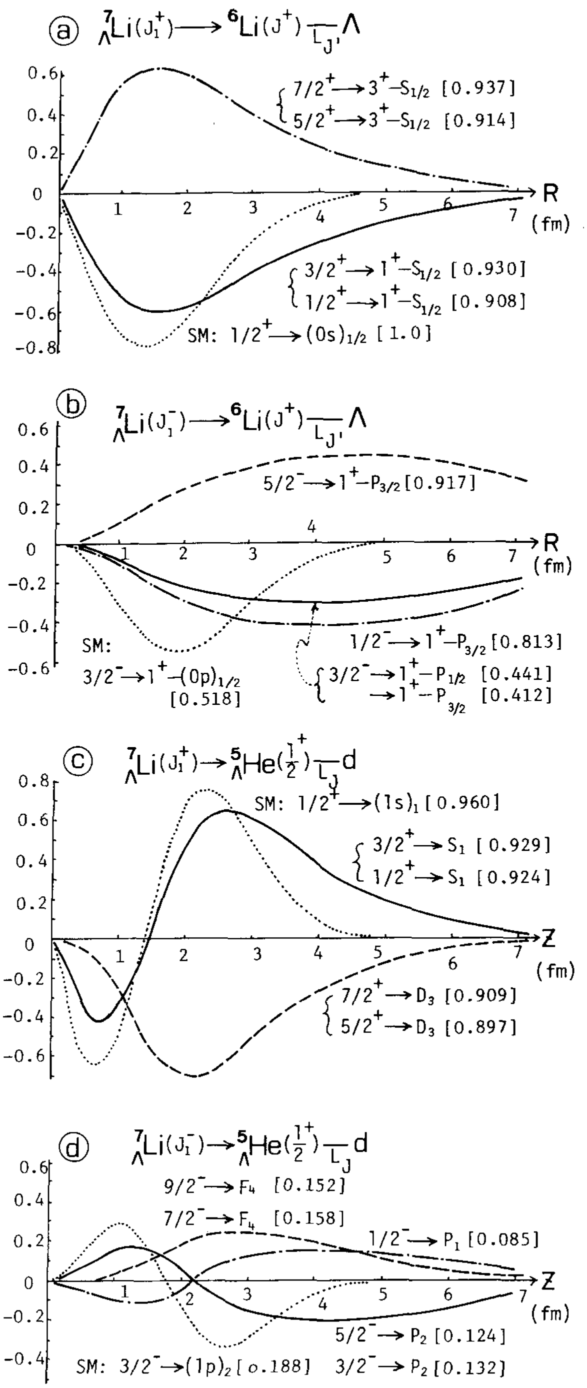

Fig. 11. RWA of $^7_\Lambda$Li. Comments as for Fig. 5.

For M1 transitions we obtain

$T(\mathrm{M1}; 3/2^+ \to 1/2^+) = 8.2 \times 10^{12}\mathrm{sec}^{-1}$;

$B(\mathrm{M1}) = 0.352\ \mathrm{nm}^2$(D-G : $0.364\ \mathrm{nm}^2$),

$T(\mathrm{M1}; 7/2^+ \to 5/2^+)$

$= 5.2 \times 10^{12}\mathrm{sec}^{-1}$;

$B(\mathrm{M1}) = 0.365\ \mathrm{nm}^2$.

See Fig. 10 for the other cases. The magnetic dipole moment of the ground state is calculated to be $\mu(1/2^+) = 0.791$ nm. The present estimates of the electromagnetic transition rates result in the lifetimes : $\tau(3/2^+) \simeq 1.2 \times 10^{-13}$sec, $\tau(5/2^+) \simeq 1.8 \times 10^{-11}$ sec and $\tau(7/2^+) \simeq 1.6 \times 10^{-13}$ sec, which are all faster than the weak decay lifetime of the free Λ particle.

Table VI lists the estimates of $B(\mathrm{E1})$ from the negative parity states of $^7_\Lambda$Li. We see that the E1 transitions occur selectively for the spin-doublet $\{1/2^-, 3/2^-\} \to 1/2^+$ and the spin-quartet $\{1/2^-, 3/2^-, 5/2^-\} \to 3/2^+$ due to their spin characters. A typical magnitude is, with 8.7 MeV, $B(\mathrm{E1}; 3/2^- \to 1/2^+) = 0.084$ $e^2\mathrm{fm}^2$. (See Fig. 10.)

Figure 11 shows the behaviors of the RWA and the spectroscopic factors for the decay processes $^7_\Lambda\mathrm{Li} \to {}^6\mathrm{Li}\text{-}\Lambda$ and $^7_\Lambda\mathrm{Li} \to {}^5_\Lambda\mathrm{He}\text{-}d$. From the partial decay width estimation shown in Table IX, we obtain $\Gamma(3/2^-) \cong 1.9 \sim 3.2$ MeV for the strong peak observed at $B_\Lambda^{\mathrm{exp}} = -2.7$ MeV in the $^7\mathrm{Li}(K^-, \pi^-)^7_\Lambda\mathrm{Li}$ reaction. See Table X for the ho expansion of the typical Λ particle wf.

4.4. *The hypernuclei $^6_\Lambda$He and $^6_\Lambda$Li*

Calculated energy spectra of $^6_\Lambda$He ($^6_\Lambda$Li) are depicted in Figs. 12 and 13. The lowest states of the core nucleus ^{5}He(^{5}Li) are $3/2^-$ and $1/2^-$, which are both unbound resonances. In the following we simply assume the same wf for both $^6_\Lambda$He and $^6_\Lambda$Li. Note that the present Λ-N interaction includes no charge-symmetry-breaking terms.

The addition of the s-state Λ particle generates the A-type (Fig. 4) negative parity hypernuclear states. The 1^--2^- and 0^--1^- pairs form the doublets with the structures

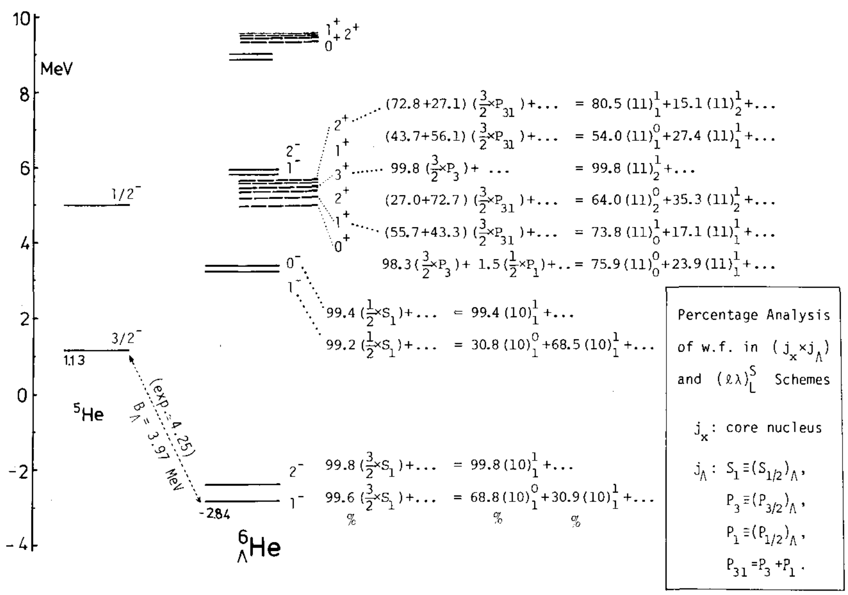

Fig. 12. Calculated energy spectra of ^{5}He and $^6_\Lambda$He($^6_\Lambda$Li). Comments as for Fig. 6.

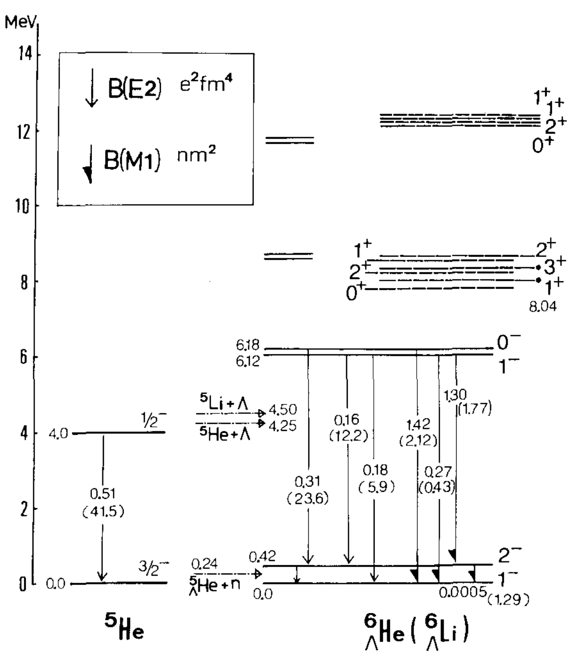

Fig. 13. Calculated B(E2) and B(M1) in ^{5}He(^{5}Li) and $^6_\Lambda$He($^6_\Lambda$Li). Comments as for Fig. 7.

$[^5\mathrm{He}(3/2^-)\times s^\Lambda_{1/2}]$ and $[^5\mathrm{He}(1/2^-)\times s^\Lambda_{1/2}]$, respectively. The order of the doublet levels is simply determined by their spin structures, because the $\boldsymbol{\sigma}_\Lambda\cdot\boldsymbol{\sigma}_N$ term acts attractively (repulsively) in the $S_<=0$ $(S_>=1)$ state. See Fig. 12 for the L-S coupling representation of the obtained wf's. The Λ particle binding energy in the ground state is calculated to be $B_\Lambda=3.97$ MeV, which is somewhat underestimated in comparison with the observed value $B_\Lambda^{\mathrm{exp}}=4.25$ MeV in $^6_\Lambda$He (4.50 MeV in $^6_\Lambda$Li).[35] This seems to be due to the limited model space adopted in treating such weakly bound states.

Available configurations for low-lying positive parity states are $(l\lambda)_L{}^S=(11)^{0,1}_{0,1,2}$, which generate two 0^+, four 1^+, three 2^+ and one 3^+ states. As seen in Fig. 12 (or 13), six of them are centered around 8 MeV excitation. Their wf's are fragmented over the possible j_x-j_Λ coupling components, indicating the recovered spatial symmetries as can be seen from the L-S coupling representation. The correspondents to the ^{6}He$(0^+, 2^+)$ and ^{6}Li$(1^+, 3^+)$ states are found in the lower group. However such an analog picture does not work well in this case. The effect of the large spin-orbit potential in ^{5}He(^{5}Li) remains as sizable mixings of different (L, S) components.

Table VII lists the calculated effective neutron numbers for the ^{6}Li$(K^-, \pi^-)^6_\Lambda$Li reaction. The N_{eff} is exclusively occupied by the $1_1{}^+$ state obtained at $B_\Lambda=-4.07$ MeV.

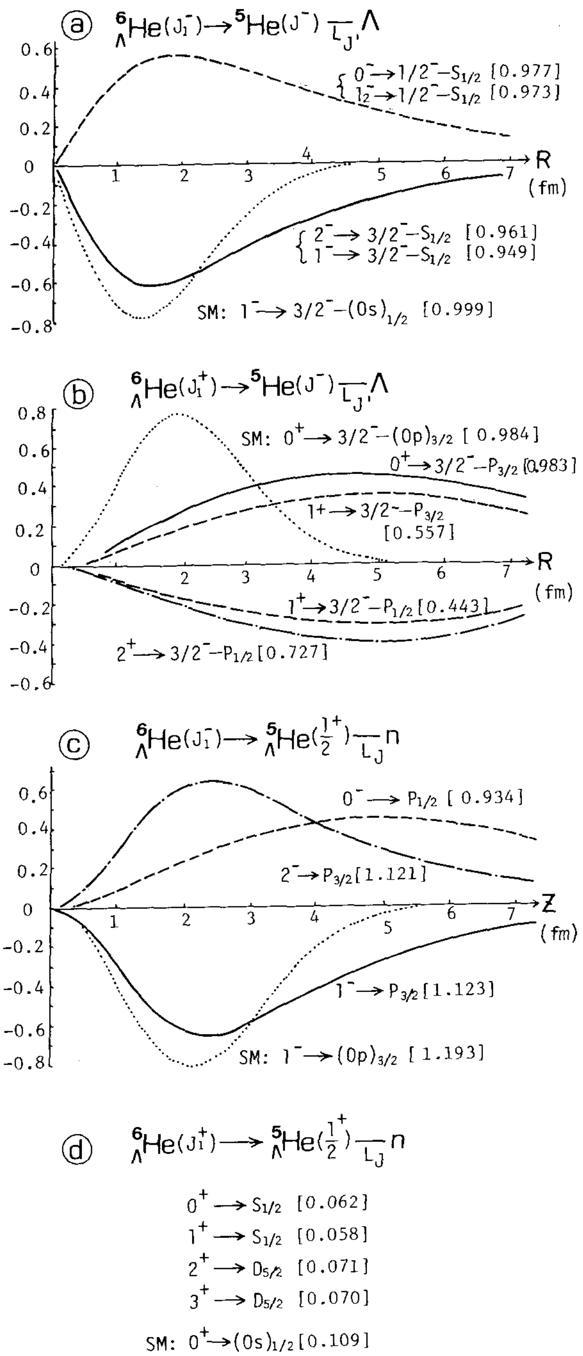

Fig. 14. RWA of ${}^6_\Lambda$He(${}^6_\Lambda$Li). Comments as for Fig. 5.

This is in good correspondece to the lower strong peak (broad resonance) observed at $B_\Lambda^{\exp}=-3.8$ MeV.[3),4)] Note that this 1_1^+ state does not have the simple shell-model substitutional structure as $(\Lambda p_{3/2},\ \nu p_{3/2}^{-1})$ but has the following character:

$$1^+=55.7\%[3/2^-\times p_{3/2}^\Lambda]+43.3\%[3/2^-\times p_{1/2}^\Lambda]+0.8\%[1/2^-\times p_{3/2}^\Lambda]+\cdots .$$

The other strong, narrow resonance peak at $B_\Lambda^{\exp}=-13.8$ MeV[3),4)] can be described by breaking the α cluster.

In Fig. 13 we summarize the calculated B(E2) and B(M1) values. Transition rates between the lowest two states of ${}^6_\Lambda$He (in parenthesis for ${}^6_\Lambda$Li) are

$$T(\mathrm{E2};\ 2^-\to 1^-)=3.67\times 10^6\ \mathrm{sec}^{-1}\quad (2.71\times 10^7\ \mathrm{sec}^{-1}),$$
$$T(\mathrm{M1};\ 2^-\to 1^-)=6.52\times 10^8\ \mathrm{sec}^{-1}\quad (1.68\times 10^7\ \mathrm{sec}^{-1}).$$

The theoretical ground-state magnetic moment is given in Table V. Table VI includes some B(E1) estimates from which we get the partial width

$$\Gamma_\gamma(1^+;\ {}^6_\Lambda\mathrm{Li})=7.2\times 10^{-6}\ \mathrm{MeV}.$$

Figure 14 illustrates the behaviors of the RWA and spectroscopic factors leading to the indicated two-body decay channels. From these we estimate the width $\Gamma(1^+)\cong 2.2\sim 3.2$ MeV for the strong peak observed at $B_\Lambda^{\exp}=-3.8$ MeV in the ^{6}Li(K^-, π^-)${}^6_\Lambda$Li reaction.[1)~5)]

§ 5. Summary

We have systematically studied the light p-shell Λ-hypernuclei, ${}^6_\Lambda$He, ${}^6_\Lambda$Li, ${}^7_\Lambda$Li, ${}^8_\Lambda$Li and ${}^9_\Lambda$Be from the cluster model point of view and have given an extensive prediction of various physical observables. These hypernuclei have been described as the microscopic $\alpha+x+\Lambda$ three-cluster system ($x=n$, p, d, t or α). The model space covers a variety of high-lying as well as important low-lying shell-model bases for the Λ particle and/or the core nucleus. The results exhibit quite rich aspects of the hypernuclear dynamics, which are generated by the participation of the Λ particle.

Table XIV. Root mean square estimates of the α-$n(p)$ and ^{5}He(^{5}Li)-Λ distances in $^6_\Lambda$He($^6_\Lambda$Li) as compared with that of ^{5}He(^{5}Li). Note that $\sqrt{\langle r^2\rangle_\alpha}=1.440$ fm with $b=1.358$ fm. (fm)

^{5}He(^{5}Li)			$^6_\Lambda$He($^6_\Lambda$Li)							
J	$\sqrt{\langle r^2\rangle_{\alpha\text{-}N}}$	Tot	J	$\sqrt{\langle r^2\rangle_{\alpha\text{-}N}}$	$\sqrt{\langle R^2\rangle_\Lambda}$	Tot	J	$\sqrt{\langle r^2\rangle_{\alpha\text{-}N}}$	$\sqrt{\langle R^2\rangle_\Lambda}$	Tot
$3/2^-$	4.12	2.09	1^-	3.46	2.51	1.96	0^+	4.19	5.04	2.70
			2^-	3.54	2.57	1.99	1^+	4.10	5.16	2.73
							2^+	4.16	5.24	2.74
							3^+	4.16	5.27	2.75
$1/2^-$	5.93	2.70	1_2^-	5.59	3.06	2.62				
			0^-	5.61	3.07	2.62				

Main results are summarized as follows:

i) The positive and negative parity energy spectra up to about 20 MeV excitation are presented for each of these hypernuclei. In all cases the present model can nicely explain existing data of B_Λ(g.s.) and B_Λ of the excited states strongly populated in the (K^-, π^-) reaction through the recoilless substitution of the last odd neutron. It is stressed that this nontrivial success is achieved as a consequence of the three-cluster dynamics.

ii) The energy levels are found to be classified into several characteristic bands (or groups) according to the underlying intrinsic structures. The addition of the $s_{1/2}$-state Λ particle to a core nucleus $(l+S_x=j_x)$ generates the corresponding doublet which can be well described with a single weak-coupling configuration $[(lj_x)\times s^\Lambda_{1/2}]_J$. The member carrying the larger $S_<=|S_x-1/2|$ component appears lower in energy than the other of the doublet. The different parity excited states with the Λ particle being dominantly in the p-state can be divided into four (two for $^9_\Lambda$Be) groups in good approximation, since, in addition to the spin $S_<$ or $S_>$, the Λ particle can move parallel (orbital $K=0$) or perpendicular $(K=1)$ to the α-x deformation axis. Thus, in the sense of the L-S coupling picture, they may be called $S_<$(or $S_>$)-analogs of the corresponding ordinary nuclear levels. Among others "genuinely hypernulear" groups are realized by virtue of the inaction of the Pauli exclusion principle on Λ.

iii) The hypernuclear γ-transition probabilities and magnetic dipole moments have been theoretically estimated. The existing data of the γ-transitions in $^7_\Lambda$Li and $^8_\Lambda$Li are in reasonable correspondence to our predictions of B(E2; $5/2^+\to1/2^+$) and B(M1; $1_2^-\to1_1^-$), respectively. In general the intra-band B(E2) values are reduced to nearly half the corresponding core nuclear ones. This is because of the sizable contraction and stablilization of the system due to the addition of the Λ particle. In spite of this fact, they remain several times enhanced in comparison with our shell-model limit values, indicating the importance of properly taking into account the clustering aspect in light hypernuclei.

iv) The reduced width amplitudes and spectroscopic factors leading to the (αx)-Λ and $^5_\Lambda$He-x decay channels have been calculated. With these, the decay widths, Γ_Λ and Γ_x, of typical levels have been estimated by using the separation energy method.

v) The application of the hypernuclear cluster model to the estimate of $N_{\rm eff}$ for the (K^-, π^-) reaction has been carried out. The results are consistent with the experiment, especially the strong peak observed at lower excitation energy.

In order to give more reliable estimates of the level widths, the bound state approximation should be improved by solving the channel-coupled scattering problem. Another improvement of the present model is to introduce intrinsic excitations of the α cluster. By this extension the other strong peak observed at the higher excitation energy in the (K^-, π^-) reaction can be described in a consistent manner. Results of these advanced treatments will be reported in the forthcoming papers.

In this paper we have presented very detailed theoretical results. The development of the hypernuclear spectroscopy is highly desired and actually being undertaken, in the light of which our predictions will have to be tested.

This work was performed as a part of the annual research project on the "Cluster Structure of Hypernuclei" in 1981~82 organized by the Research Institute for Fundamental Physics, Kyoto University. We are thankful to Professor H. Horiuchi, Professor H. Ejiri and Professor F. Takeuchi for their valuable comments and discussions. One of the authors (H.B.) was partly supported by a "Grant-in-aid for Scientifc Research of Ministry of Education, Science and Culture".

Numerical computations were carried out at the Data Processing Center of Kyoto University.

Appendix

The folding potential U_J^{AN} between the Λ particle and the $\alpha+x$ core nucleus is defined by Eq. (2·10). The explicit form for the Gaussian Λ-N interaction of Eq. (2·22) is given in terms of the spherical Bessel function with an imaginary arguement, $\mathcal{J}_k$:

$$U_J^{AN}(c_1d_1K_1,\ c_2d_2K_2)=\delta(L_1S_1,\ L_2S_2)\cdot\langle u_{K_1\lambda_1}(R)|U_{L_1S_1}(l_1\lambda_1d_1,\ l_2\lambda_2d_2)|u_{K_2\lambda_2}(R)\rangle,$$

$$c\equiv\{l,\lambda,L,S\}, \tag{A·1}$$

$$\begin{aligned}
U_{LS}(l_1\lambda_1d_1,\ l_2\lambda_2d_2)=&F_1(S,x)\cdot 4\pi v^0_{\Lambda N}\left(\frac{\beta_{\Lambda N}}{\Gamma}\right)^3\sum_{k_1k_2k_3k_4}(-)^L\sqrt{[\lambda_1][\lambda_2]}(\lambda_10\lambda_20|k_40)\\
&\times W(l_1\lambda_1l_2\lambda_2;\ Lk_4)(-)^{k_3+l_2+k_4}[k_1][k_2][k_3](k_10k_20|l_10)(k_10k_30|l_20)(k_20k_30|k_40)\\
&\times W(l_1k_2l_2k_3;\ k_1k_4)\cdot\exp[-A(d_1^2+d_2^2)/4b^2-(R^2/\Gamma^2)]\\
&\times\Bigg[F_2(x)\cdot\sum_{y=0}^{x}\frac{x!}{y!(x-y)!}(-)^y\\
&\quad\times\exp[-\nu_\alpha^2(d_1^2+d_2^2)/4\Gamma^2]\cdot\mathcal{J}_{k_1}(p_1(y)d_1d_2)\ \mathcal{J}_{k_2}(-q_\alpha d_1R),\ \mathcal{J}_{k_3}(-q_\alpha d_2R)\\
&+F_3(x)\cdot\sum_{y=0}^{x-1}\frac{(x-1)!}{y!(x-1-y)!}(-)^y\\
&\quad\times\{\exp[-\nu_\alpha^2(d_1^2+d_2^2)/4\Gamma^2]\cdot\mathcal{J}_{k_1}(p_1(y)d_1d_2)\ \mathcal{J}_{k_2}(-q_\alpha d_1R)\ \mathcal{J}_{k_3}(-q_\alpha d_2R)\\
&\quad+\exp[-\nu_x^2(d_1^2+d_2^2)/4\Gamma^2]\cdot\mathcal{J}_{k_1}(p_2(y)d_1d_2)\ \mathcal{J}_{k_2}(q_xd_1R)\ \mathcal{J}_{k_3}(q_xd_2R)\\
&\quad-\exp[-(\nu_\alpha^2d_1^2+\nu_x^2d_2^2)/4\Gamma^2]\cdot\mathcal{J}_{k_1}(p_3(y)d_1d_2)\ \mathcal{J}_{k_2}(-q_\alpha d_1R)\ \mathcal{J}_{k_3}(q_xd_2R)\\
&\quad-\exp[(-(\nu_x^2d_1^2+\nu_\alpha^2d_2^2)/4\Gamma^2]\cdot\mathcal{J}_{k_1}(p_3(y)d_1d_2)\ \mathcal{J}_{k_2}(q_xd_1R)\ \mathcal{J}_{k_3}(-q_\alpha d_2R)\}\Bigg],
\end{aligned} \tag{A·2}$$

$$\nu_a \equiv \frac{x}{4+x}, \quad \nu_x \equiv \frac{4}{4+x}, \quad A \equiv 4\nu_a^2 + x\nu_x^2, \tag{A·3a}$$

$$\Gamma^2 \equiv \beta_{\Lambda N}^2 + \left(1 - \frac{1}{4+x}\right) b^2, \tag{A·3b}$$

$$p_1(y) = (A-y)/2b^2 - \nu_a^2/2\Gamma^2, \tag{A·3c}$$

$$p_2(y) = (A-y)/2b^2 - \nu_x^2/2\Gamma^2, \tag{A·3d}$$

$$p_3(y) = (A-y-1)/2b^2 + \nu_a\nu_x/2\Gamma^2, \tag{A·3e}$$

$$q_a = \nu_a/\Gamma^2, \qquad q_x = \nu_x/\Gamma^2. \tag{A·3f}$$

In the above expression the factors are $F_1(S, x) = 1$, $F_2(x) = 4 - x$ and $F_3(x) = x$ for the Wigner part folding potential, and for the $\boldsymbol{\sigma}_\Lambda \cdot \boldsymbol{\sigma}_N$ part

$$F_1(S, x) = \begin{cases} \eta(4S-3) & \text{for } x = 1 \text{ or } 3, \\ \eta(6S-7) & \text{for } x = 2, \\ 0 & \text{for } x = 4, \end{cases}$$

$F_2(x) = -1$ and $F_3(x) = 1$.

References

1) W. Brückner et al. (Heidelberg-Saclay-Strasbourg Collaboration), Phys. Lett. **55B** (1975), 107; **62B** (1976), 481; **79B** (1978), 157.
2) R. Bertini et al. (H-S-S Collaboration), Phys. Lett. **83B** (1979), 306; **90B** (1980), 375.
3) R. Bertini et al. (H-S-S Collaboration), Nucl. Phys. **A360** (1981), 315.
4) R. Bertini et al. (H-S-S Collaboration), Nucl. Phys. **A368** (1981), 365.
5) B. Povh, Rep. Prog. Phys. **39** (1976), 824; Ann. Rev. Nucl. Part. Sci. eds. J. D. Jackson et al. (1978, Annual Reviews Inc., Palo Alto), p. 1; J. Phys. Soc. Japan Suppl. **44** (1978) p. 775; Nucl. Phys. **A335** (1980), 233; Prog. Part. Nucl. Phys. **5** (1981), 245.
6) R. E. Chrien, M. May, H. Palevsky, R. Sutter, P. Barnes, S. Dytman, D. Marlow, F. Takeuchi, M. Deutch, R. Cester, S. Bart, E. Hungerford, T. M. Williams, L. S. Pinsky, B. W. Mayes and R. L. Stears, Phys. Lett. **89B** (1979), 31.
7) M. May et al. Phys. Rev. Lett. **47** (1981), 1106.
8) M. Bedjidian et al. (CERN-Lyon-Warsaw Collaboration), Phys. Lett. **94B** (1980), 480.
9) M. May, *Proc. Inter. Conf. on Hypernuclear and Kaon Physics* (1982, Heidelberg), ed. B. Povh, p. 63.
H. Piekarz, ibid, p. 73.
M. Deutsch et al. (MIT-BNL-Houston-CMU-New Mexico-Vassar Collaboration), to be published.
10) D. H. Davis and J. Sacton, in *High Energy Physics,* Vol. II, ed. E. H. S. Burhop (1967, Academic Press), p. 365.
11) A. Gal, J. M. Soper and R. H. Dalitz, Ann. of Phys. **63** (1971) 53; **72** (1972), 445; **113** (1978), 79.
12) J. Hüfner, S. Y. Lee and H. A. Weidenmüller, Nucl. Phys. **A234** (1974), 429; Phys. Lett. **49B** (1974), 409.
13) A. Gal, *Advances in Nucl. Phys.*, eds. M. Baranger and E. Vogt, Vol. 8 (1975, Plenum, New York), p. 1.
14) A. Bouyssy, Nucl. Phys. **A290** (1977), 324.
15) R. H. Dalitz and A. Gal, Ann. of Phys. **116** (1978), 167.
16) R. H. Dalitz, *Proc. Int. Conf. Nuclear Structure* (1980, Berkeley), Nucl. Phys. **A354** (1981), 101c.
17) C. B. Dover, *Proc. 9th Int. Conf. High Energy Physics and Nuclear Structure* (1981, Versailles), Nucl. Phys. **A374** (1982), 359c.
C. B. Dover and G. E. Walker, Phy. Rep. **89**, No. 1 (1982), 1.
18) H. Bandō, INS-PT-31(1982), INS, University of Tokyo.
19) A part of this work has been reported previously:
T. Motoba, H. Bandō and K. Ikeda, *Proc. Inter. Conf. on Hypernuclear and Kaon Physics* (1982, Heidelberg), ed. B. Povh, p. 129.
Some figures and the table appeared in the report are partly corrected in the present paper.
20) Zhang Zong-ye, Li Guang-lie and Shen Jian-ping, *Transactions of the New York Academy of Sciences* **II-40** (1980), p. 274.
Zhang Zong-ye, Li Guang-lie and Yu You-wen, Phys. Lett. **108B** (1982), 261.

21) R. H. Dalitz and A. Gal, Phys. Rev. Lett. **36** (1976), 362; Ann. of Phys. **131** (1981), 314.
22) L. Majling, M. Sotona, J. Žofka, V. N. Fetisov and R. A. Eramzhyan, Phys. Lett. **92B** (1980), 256.
23) E. H. Auerbach, A. J. Baltz, C. B. Dover, A. Gal, S. H. Kahana, L. Ludeking and D. J. Millener, Phys. Rev. Lett. **47** (1981), 1110.
24) R. H. Dalitz and G. Rajasekaran, Nucl. Phys. **50** (1964), 450.
25) A. R. Bodmer and S. Ali, Nucl. Phys. **56** (1964), 657.
26) A. R. Bodmer and J. W. Murphy, Nucl. Phys. **64** (1965), 593; **73** (1965), 664.
27) Y. C. Tang and R. C. Herndon, Phys. Rev. **138** (1965), B637.
28) Y. C. Tang and R. C. Herndon, Nuovo Cim. **66** (1966), 117.
29) J. Revai and J. Žofka, Phys. Lett. **101B** (1981), 228.
30) Y. Sunami and H. Narumi, Prog. Theor. Phys. **66** (1981), 355.
31) H. Bandō, M. Seki and Y. Shono, Prog. Theor. Phys. **66** (1981), 1218; **68** (1982), 364.
32) K. Ikeda et al., Prog. Theor. Phys. Suppl. No. 52 (1072); No. 68 (1980).
33) For example, *Proc. Int. Conf. Clustering Aspects of Nuclear Structure and Nuclear Reactions* (1978), Winnipeg), ed. W. T. H. Van Oers et al. (AIP Conf. Proc. No. 47).
34) D. L. Hill and J. A. Wheeler, Phys. Rev. **89** (1953), 1106.
J. J. Griffin and J. A. Wheeler, Phys. Rev. **108** (1957), 311.
K. Ikeda et al., Prog. Theor. Phys. Suppl. No. 62 (1977).
35) The compilations quoted in Ref. 13).
36) S. Saito, Prog. Theor. Phys. **40** (1968), 893; **41** (1969), 705.
37) H. Nishioka, S. Saito and M. Yasuno, Prog. Theor. Phys. **62** (1979), 424.
38) For example, N. K. Glendenning, Phys. Rev. **137** (1965), B102.
39) H. Horiuchi, K. Ikeda and Y. Suzuki, Prog. Theor. Phys. Suppl. No. 52 (1972), Chap. III, p. 89.
40) R. H. Dalitz and A. Gal, Phys. Lett. **64B** (1976), 154.
41) A. Bouyssy, Phys. Lett. **84B** (1979), 41; **99B** (1981), 373.
42) S. Okabe, Y. Abe and H. Tanaka, Prog. Theor. Phys. **57** (1977), 866.
43) H. Bandō, K. Ikeda and T. Motoba, Prog. Theor. Phys. **69** (1983), 918.